Meteorol Atmos Phys (2016) 128:1–22
DOI 10.1007/s00703-015-0405-1

ORIGINAL PAPER

A comparative study of the role of the Saharan air layer in the evolution of two disparate Atlantic tropical cyclones using WRF model simulations and energetics calculations

Robert S. Ross[1] · **T. N. Krishnamurti**[1] · **Kirsten M. Chaney**[1]

Received: 31 March 2015 / Accepted: 14 September 2015 / Published online: 24 September 2015

Abstract The Weather Research and Forecasting (WRF) Model 5-day simulations of Major Hurricane Julia (2010) and Tropical Storm Florence (2012), both of which developed from African easterly waves, are used to conduct a complete energetics study to explain why one storm became a major hurricane while the other weakened to a wave. The disparate intensity outcomes are caused by significant differences in the energetics of the two systems that emerge in their storm stages due to differences in the impact of the Saharan air layer (SAL). In their wave stages both waves exhibit a convectively driven energy production cycle, in which the regions of positive barotropic and baroclinic energy conversion and of diabatic heating and rainfall are all superimposed. Convection induces barotropic instability which then enhances the baroclinic overturning through a resonance of the two instabilities, which together produce the eddy kinetic energy. Diabatic heating in the convection generates eddy available potential energy which, along with the eddy kinetic energy, defines the total eddy energy of the system. Florence loses the convectively driven energy production cycle in the storm stage and begins to weaken, while Julia maintains this cycle and becomes a major hurricane. The disruption of the convection in Florence is due to the drying, stabilizing, and vertical shearing effects of an expansive SAL to the north of the storm, effects not present in the Julia case. Consideration is given to the different effects of the SAL on 6–10 day waves (Florence wave) versus 3–5 day waves (Julia wave).

Responsible Editor: M. Kaplan.

✉ Robert S. Ross
rross@fsu.edu

[1] Earth, Ocean, and Atmospheric Science, The Florida State University, Tallahassee, FL 32306-4520, USA

1 Introduction

African easterly waves (AEWs) have been studied for over four decades with a variety of observational and numerical approaches, beginning with the studies by Carlson (1969), Burpee (1972), Reed et al. (1977), and Norquist et al. (1977). These waves have been shown to be instrumental in the formation of Atlantic tropical cyclones in studies by Riehl (1954), Thorncroft and Hodges (2001), Frank (1970), and Avila et al. (2000).

The causes and dynamics of AEWs are topics of ongoing research. Many studies have associated the waves with hydrodynamic instability of the African easterly jet (AEJ) located near 600 hPa and 15N over Africa and the Atlantic in summer (Burpee 1972; Rennick 1976; Kwon 1989; Thorncroft et al. 1994a, 1994b). Strong shear to the south of the jet is associated with a reversal in the meridional gradient of isentropic potential vorticity (IPV) implying that the jet may be hydrodynamically unstable according to the criteria for combined barotropic-baroclinic instability of Charney and Stern (1962) and Fjortoft (1950). Other studies have focused on the role of diabatic heating within the ITCZ as a cause for the waves (Holton 1971; Estoque and Lin 1977; Schubert et al. 1991; Hsieh and Cook 2005). Strong and organized convection in the ITCZ can lead to a reversal of the mid-tropospheric IPV gradient, and therefore, to combined barotropic–baroclinic instability without the presence of the AEJ.

Numerical weather prediction (NWP) and climate models provide an excellent tool for studying the structure

and dynamics of AEWs, including their energetics. Such models can simulate the wave dynamics and energetics with a time and space resolution that is not possible with existing observational systems and re-analyses. Hsieh and Cook (2007) used a regional climate model to conduct a complete energetics study of AEWs occurring during the climatological period of 15 May to 14 September. In their paper, and in a follow-up paper (Hsieh and Cook 2008), the authors found that the waves were initiated by the diabatic heating in the ITCZ rather than by the hydrodynamic instability of the AEJ, confirming their earlier findings in Hsieh and Cook (2005).

A very important factor in the understanding of AEWs and their evolution into tropical cyclones over the tropical North Atlantic is the presence of the Saharan air layer (SAL), a region of warm, dry air which originates over the desert regions of North Africa in summer and is found as an elevated well-mixed layer over the Atlantic extending from 900 to 500 hPa, with the mid-level AEJ located along its southern boundary. Determination of the role of the SAL in Atlantic cyclogenesis is a major goal of NASA's Hurricane and Severe Storm Sentinel (HS3) Project whose field phase was conducted in the Atlantic during the summers of 2012–2014. Dunion and Velden (2004) found that the SAL appears to suppress tropical cyclone activity by: ingesting dry, stable air into the circulation which promotes evaporation and convectively driven downdrafts; dramatically enhancing the local vertical wind shear through the presence of the AEJ; enhancing the pre-existing trade wind inversion, further stabilizing the environment. Karyampudi et al. (2002) found that the SAL enhanced the development of two Atlantic storms but had a negative impact on a third storm. Several examinations of the SAL have included modeling studies of the dust-radiation effects on parameters such as temperature, moisture, and the vertical wind shear (e.g. Chen et al. 2010). Other studies have considered how the cloud hydrometeors may be affected by the dust, in addition to inclusion of the dust-radiation effects (e.g. Zhang et al. 2009; Rosenfeld et al. 2012).

The aim of the present study was to compare the evolution of two Atlantic storms, major Hurricane Julia (2010) and Tropical Storm Florence (2012), from AEWs, with a focus on the impact of the SAL. The findings will be based on direct examination of high-resolution (6 km) WRF model 5-day simulations of the two storms and on the results of a complete energetic study of the two storms using parameters from the high-resolution WRF model runs. After a careful examination of the two precursor AEWs to determine if there were significant differences in their structures and energetics that may have contributed to the strikingly different tropical cyclones that they produced, the study turns to its primary focus which is an assessment of the key role played by the SAL in the very different outcomes for the two storms. Section 2 will describe the WRF model and the energetics equations used in the study. After a brief synoptic history of Julia and Florence in Sect. 3, Sects. 4 and 5 will present the results of the detailed energetics study of the two storms. Section 6 will assess the critical role that the SAL played in defining the different energetics patterns in the two storms to explain their very different intensity outcomes, and Sect. 7 will present the salient conclusions of the study.

2 Methodology

2.1 WRF-ARW model

The WRF-ARW Version 3 numerical model was used to make 5-day simulations for Julia and Florence. The model domain is shown in Fig. 1 along with the NHC best track for each system during the 5-day model simulations. The domain extends from 5 to 30N and 10 to 55W which keeps the storms well away from the boundaries and provides an appropriately large domain for the energetics calculations. Initial and boundary conditions are provided by the GFS (Global Forecast System) FNL (final) analysis. The vertical resolution is 50 hPa with 19 levels extending from 1000 to 100 hPa. Output was archived for every 3 h during the forecast period. Numerous experiments were conducted with a variety of grid resolutions and cumulus parameterization schemes, and a single domain with a 6-km grid resolution and no cumulus scheme was found to give the best simulations for the two storms, although a 6-km grid may be border line as far as the explicit simulation of clouds.

For this study the WRF model was configured with the following physics schemes: microphysics [Lin (Purdue)]; long-wave radiation (RRTM); short-wave radiation (Dudhia); surface layer (Eta similarity); surface (Unified Noah land-surface model); planetary boundary layer (Mellor-Yamada-Janjic).

2.2 Energetics calculations

The generation and maintenance of tropical disturbances can be understood through a diagnosis of their energy processes. Using the high-resolution model output, energetics calculations were carried out for the two tropical systems, based on the foundational work of Lorenz (1955), Oort (1964), and Norquist et al. (1977). The calculations include a complete analysis of all partitioned energies, energy conversions, generation and dissipation terms, and boundary fluxes, as in the study by Hsieh and Cook (2007).

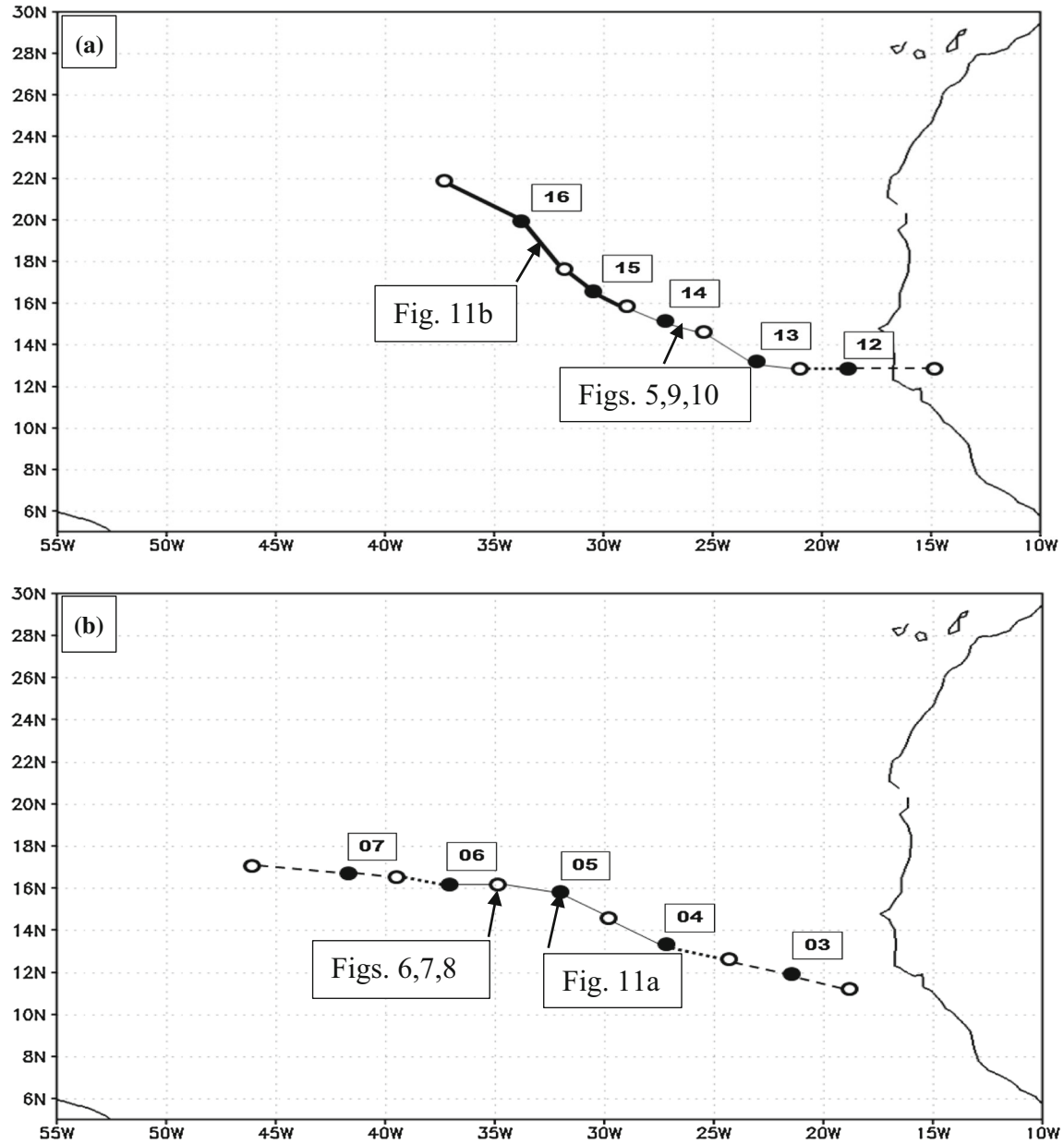

Fig. 1 The domain used for the WRF model simulations and the energetics calculations along with National Hurricane Center best track plots for **a** Julia from 1200 UTC 11 September 2010 to 1200 UTC 16 September 2010, and **b** Florence from 1200 UTC 02 August 2012 to 1200 UTC 07 August 2012. *Darkened circles* indicate positions for 0000 UTC on the day indicated in the *box* by each *darkened circle* and *open circles* indicate positions at 1200 UTC. *Dashed line* (wave), *dotted line* (depression), *thin solid line* (tropical storm), *thick solid line* (hurricane). Locations for figures referred to in the text are indicated along the track plots

The governing equations for eddy kinetic and eddy available potential energy in an open system are given by Eq. (1) and Eq. (2), respectively.

$$\frac{\partial K_{\mathrm{E}}}{\partial t} = C_{\mathrm{k}} + C_{\mathrm{pk}} - D_{\mathrm{E}} + K_{\mathrm{EB}} + \Phi_{\mathrm{EB}}, \tag{1}$$

$$\frac{\partial A_{\mathrm{E}}}{\partial t} = C_{\mathrm{A}} - C_{\mathrm{pk}} + G_{\mathrm{E}} + A_{\mathrm{EB}} \tag{2}$$

The mathematical expressions for all variables and terms are given in the appendix. Variable K_{E} is the eddy kinetic energy [Eq. (6)], and A_{E} is the eddy available potential energy [Eq. (7)], both averaged over the domain. The barotropic energy conversion,C_{k}, includes the sum of four terms [C_{k1} through C_{k4} in Eq. (8)] which treat the conversion of zonal to eddy kinetic energy through the zonal (u) and meridional (v) wind shears. The baroclinic conversion of eddy available

potential energy to eddy kinetic energy is represented by C_{pk} [Eq. (9)]. The conversion of zonal available potential energy to eddy available potential energy due to eddy heat flux along the zonal mean temperature gradient is given by C_A [Eq. (10)]. The generation of eddy available potential energy by diabatic heating is represented by G_E [Eq. (11)], where positive generation occurs when warmer regions are heated and colder regions are cooled at the same latitude. Frictional dissipation of eddy kinetic energy is given by D_E [Eq. (12)]. K_{EB} and A_{EB} represent boundary fluxes of eddy kinetic and eddy available potential energy, respectively, into or out of the calculation domain [Eqs. (13, 15)], and Φ_{EB} [Eq. (14)] represents boundary pressure work done by eddies.

3 Brief synoptic history of Major Hurricane Julia (2010) and Tropical Storm Florence (2012)

The AEW that developed into Hurricane Julia emerged from the West African coast around 1200 UTC 11 September 2010, which is the time it was initialized in the WRF model. (See Fig. 1a). A depression formed by 0600 UTC 12 September, and a tropical storm formed shortly thereafter at 1800 UTC 12 September. After a rather long period as a tropical storm, Julia intensified into a hurricane on 1200 UTC 14 September, and then rapidly intensified into a major hurricane just 18 h later at 0600 UTC 15 September. Peak intensity of 948 hPa and 120 knots (category 4 storm) was reached on 1200 UTC 15 September, and major hurricane status was maintained through 1200 UTC 16 September, which is the end of the WRF model 5-day simulation. The genesis of Julia from a strong AEW has been the subject of a number other investigations, e.g. Cecelski and Zhang (2013, 2014).

The AEW that developed into Tropical Storm Florence departed the West African coast around 1200 UTC 2 August 2012 which is the time it was initialized in the WRF model (See Fig. 1b). A tropical depression formed by 1800 UTC 3 August, which rather quickly developed into a tropical storm by 0600 UTC 4 August. Florence remained a tropical storm until around 0600 UTC 6 August and during this period attained peak intensity of 1002 hPa and 50 knots at 0000 UTC 5 August. The system deteriorated into a depression by 0600 UTC 6 August and then into a wave 6 h later, a status that it maintained until the end of the model simulation on 1200 UTC 7 August.

The WRF model developed the Julia system from a wave to a hurricane with peak intensity of 970 hPa and 80 knots (compared to 948 hPa and 120 knots in the best track), and the Florence system from a wave to a tropical storm with peak intensity of 998 hPa and 60 knots (compared to 1002 hPa and 50 knots in the best track). These simulations are considered to be adequate to capture the key dynamical processes in the two storms, so that a meaningful assessment of the causes of their radically different outcomes can be analyzed through parameter mapping and energetics calculations.

4 Initial results of energetics calculations for Julia and Florence: energy cycle diagrams and tables of energetics parameters

This section will primarily seek to determine if there were significant differences in the energetics of the two precursor AEWs that may offer clues as to why one wave developed into a major hurricane while the other wave became a tropical storm only to weaken back to the wave stage. A complete energetics study was conducted for both storms utilizing the equations in the appendix. Time series plots of all terms were constructed for the 5-day simulations, and energy cycle diagrams were constructed for the full 5-day period and for each of the sub-classifications of each system: wave, depression, storm, hurricane for Julia; wave, depression, storm, dissipation for Florence. The products presented here will deal primarily with the genesis of the two systems from wave to tropical storm.

Figure 2 shows the energy cycle diagrams for the precursor waves of Julia and Florence. The energy cycles are in good agreement with those of Norquist et al. (1977) and Hsieh and Cook (2007) with a few exceptions. For both waves the eddy kinetic energy is primarily maintained by the baroclinic conversion term, C_{pk}, with the barotropic conversion term, C_k, being a secondary source, as in the earlier studies. Hsieh and Cook found that A_E was maintained by C_A and G_E in an approximate 2–1 ratio. In the present study A_E is maintained by these two energy sources, but G_E dominates C_A, particularly for the Julia wave. The eddy energies are larger compared to their respective zonal energies than in the two earlier studies, particularly for the Florence wave, and this may be due to the very small grid size (6 km) used in this study. Both Φ_{EB} and K_{EB} remove eddy kinetic energy from the domain as in Hsieh and Cook, but the values are much larger here, particularly for the Florence wave, where the large values were traced to a pronounced upper tropospheric trough in the far northwest corner of the domain. This trough was far removed from Florence and was not responsible for its relative lack of development.

It is very important for the current study to note that the energy cycles are largely comparable for the two waves. This is our first evidence that the radically different outcomes for Julia and Florence were not due to significant differences in their initiating waves. For both waves the eddy kinetic energy is primarily maintained by the baroclinic conversion term, C_{pk}, and the eddy available

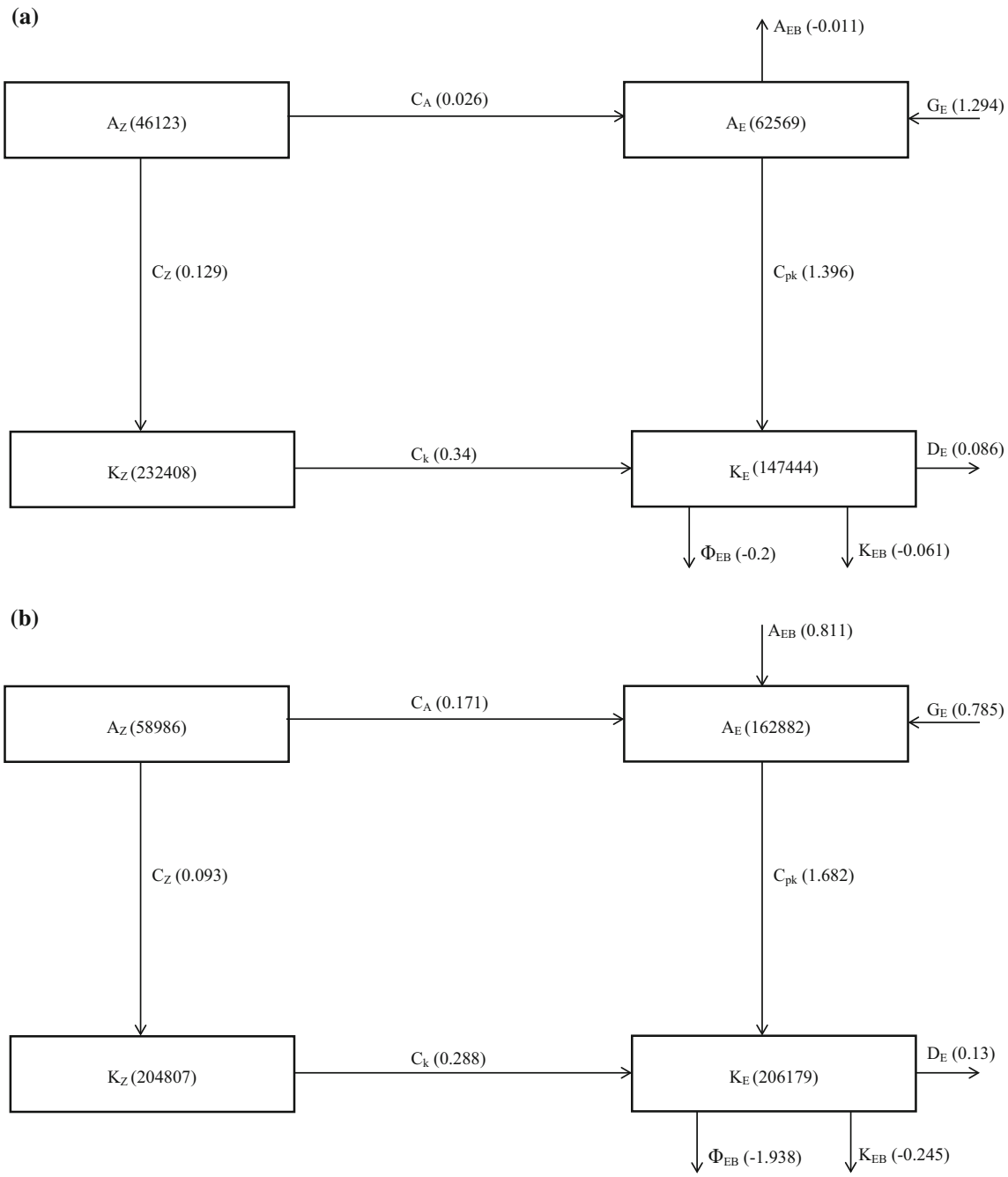

Fig. 2 Partitioned energies (J m^{-2}) and energy conversion rates (W m^{-2}) for the wave stage of **a** Julia and **b** Florence

potential energy is maintained primarily by diabatic heating through the generation term, G_E.

Tables 1, 2, 3, and 4 allow for a succinct evaluation of how the energetics of the two disturbances change as each system strengthens from wave to depression to storm stages. The pertinent contributors to changes in the eddy energy, along with the doubling time for that energy, are provided. Tables 1 and 2 present this information for the eddy kinetic energy and the total eddy energy, respectively,

Table 1 Doubling time (days) for eddy kinetic energy for Julia in three intensity categories, along with eddy kinetic energy values (J m^{-2}) and energy conversion components (W m^{-2})

	C_k	C_{pk}	$-D_E$	K_E	Doubling time
Wave	0.340	**1.396**	0.086	**147444**	1.03
Depression	0.247	**1.857**	0.099	**182982**	1.06
Storm	0.216	**3.060**	0.055	**255756**	0.92

Table 2 Doubling time (days) for the total eddy energy for Julia in three intensity categories, along with total eddy energy values (J m^{-2}) and energy conversion components (W m^{-2})

	C_A	G_E	C_k	$-D_E$	$A_E + K_E$	Doubling time
Wave	0.026	**1.294**	0.340	0.086	**210013**	1.54
Depression	−0.020	**1.901**	0.247	0.099	**243538**	1.39
Storm	−0.048	**3.003**	0.216	0.055	**331561**	1.23

Table 3 Doubling time (days) for eddy kinetic energy for Florence in three intensity categories, along with eddy kinetic energy values (J m^{-2}) and energy conversion components (W m^{-2})

	C_k	C_{pk}	$-D_E$	K_E	Doubling time
Wave	**0.288**	**1.682**	0.130	**206179**	1.30
Depression	**0.318**	**1.801**	0.125	**201066**	1.17
Storm	**−0.046**	**1.105**	0.111	**170577**	2.08

for Julia. Tables 3 and 4 do likewise for Florence. Doubling time is defined as the average energy in the domain, divided by the summation of the contributors to changes in that energy, and indicates the number of days required for the energy to double. The numbers that are most important for understanding the energetics patterns are indicated in bold.

In Table 1 the eddy kinetic energy for Julia is seen to increase steadily from wave to storm (numerator in the doubling time calculation), yet the doubling time remains close to one day for each category. This occurs because the baroclinic conversion term, C_{pk} (denominator in the doubling time calculation), nearly triples from wave to storm. This shows the importance of baroclinic overturning for Julia's genesis. The barotropic conversion term, C_k, decreases slightly from wave to storm, but remains positive. In Table 2 the total eddy energy for Julia is likewise seen to steadily increase from wave to storm, while the doubling time drops from 1.54 to 1.23 days. This happens largely because of the near tripling of the generation term, G_E. This shows the importance of diabatic heating, largely in convection, for Julia's genesis. These two energy sources work in tandem, as rising warm air builds the positive C_{pk} term and supports the convection.

For Florence the energetics patterns from wave to storm are more complex as revealed in Table 3 (eddy kinetic energy) and Table 4 (total eddy energy). The eddy kinetic energy decreases slightly from wave to depression, while the doubling time also decreases. This is consistent with slight increases in the baroclinic conversion, C_{pk}, and the barotropic conversion, C_k, as both conversions maintain values that are close to, or even larger than, the values for Julia. But from the depression to the storm stage, the eddy kinetic energy drops noticeably as the doubling time almost doubles from 1.17 to 2.08 days. This happens because the baroclinic conversion, C_{pk}, and the barotropic conversion, C_k, both decrease during this period, particularly the barotropic conversion, which becomes negative by the storm stage. The two sustaining energy conversion terms for eddy kinetic energy, which were robust during the wave stage, are disintegrating, and this is consistent with Florence's lack of continued development beyond the storm stage. The total eddy energy for Florence (Table 4) is larger than for Julia in the wave and depression stages but drops below Julia's values in the storm stage. This energy drops slightly from wave to depression stages in Florence, as the doubling time nearly doubles from 3.83 to 6.28 days due to the roughly halving of the generation term, G_E, which was already about two times smaller than in Julia. From the depression to the storm stage, the total eddy energy drops more noticeably, as the doubling time jumps to a huge value of 16.99 days due to the reversal of both the C_A and C_k terms from positive to negative values.

Florence is actually stronger as a wave than Julia with regard to both eddy kinetic energy and total eddy energy. As a depression Florence still exceeds the Julia depression in both forms of energy but by diminishing amounts. It is not until the storm stage that Julia begins to surpass Florence in both energies.

In summary, the different outcomes for the Julia and Florence systems cannot be explained by differences in

Table 4 Doubling time (days) for the total eddy energy for Florence in three intensity categories, along with total eddy energy values (J m^{-2}) and energy conversion components (W m^{-2})

	C_A	G_E	C_k	$-D_E$	$A_E + K_E$	Doubling time
Wave	0.171	**0.785**	0.288	0.130	**369061**	3.83
Depression	**0.114**	**0.348**	**0.318**	0.125	**355596**	6.28
Storm	**−0.145**	0.501	**−0.046**	0.111	**292041**	16.99

their energetics during the wave and depression stages. Florence is actually more energetic than Julia in these stages, and both systems are maintained by barotropic and baroclinic conversions, with the latter being dominant. Both systems are energized by diabatic heating through the generation term, although for Julia this generation is at least twice as large as for Florence. It is in the storm stage that Florence begins to show significant differences from Julia in the energetics patterns. Florence's eddy kinetic energy and total eddy energy fall below Julia's, as C_{pk} decreases, C_k and C_A both become negative, and, very significantly, the generation term in Florence, which was already lagging behind Julia's, drops to about one-sixth of that in Julia in the storm stage (0.501W m^{-2} versus 3.003W m^{-2} in Tables 4, 2, respectively). The remainder of this paper will seek to explain why these differences in energetics patterns occur and why Julia continues to strengthen while Florence weakens.

5 Further results of energetics calculations for Julia and Florence: spatial distributions of energetics parameters

This section extends the results of the previous section through vertical cross-sections and horizontal maps of energetics patterns. These results provide a clearer picture of the energetics patterns for the two storms and lay the groundwork for explaining why those energetics patterns become significantly different with time, resulting in radically different storms.

Four six-panel figures will be used to convey the energetics patterns. Each figure depicts (a) a meridional profile of u-wind, (b) a vertical section of IPV, (c) the integrand for term C_{k1} in Eq. (8) (barotropic conversion), (d) the integrand for term C_{pk} in Eq. (9) (baroclinic conversion), (e) diabatic heating ($Q = c_p T\theta^{-1} d\theta dt^{-1}$), (f) WRF model rain. The caption gives specific details on how each panel is constructed. Figures 3 and 4 are for the wave stages of Julia and Florence, respectively, while Figs. 5 and 6 are for the storm stages of Julia and Florence, respectively. For convenience in interpretation, the maximum value of the parameter is indicated in each panel. Arrows are used to focus attention on difficult to see patterns. The time of each figure in relation to the storm's evolution is indicated along the best track plots in Fig. 1.

The energetics patterns for the Julia wave (Fig. 3) and for the Florence wave (Fig. 4) are quite similar, further confirming the earlier conclusion that the ultimate difference in the storms' intensity could not be traced to significant differences in their wave and depression stages. The various maximum values of parameters are equal in the two systems, or even a bit larger in Florence: IPV, 4e-06 (J) and 6e-06 (F); barotropic conversion integrand, 0.002 (J) and 0.006 (F); baroclinic conversion integrand, 180 (J) and 220 (F); diabatic heating, 50 (J) and 45 (F); model rain, 240 (J) and 220 (F). For both waves there is a complex region of maximum IPV centered near 11N with a sign reversal in the meridional IPV gradient indicated by shading. It is not possible in this study to decipher whether the combined barotropic-baroclinic instability implied by this sign reversal is due primarily to hydrodynamical instability of the AEJ or to diabatic heating in ITCZ convection. The sign reversal does occur in a region of strong horizontal wind shear to the south of the AEJ (see panel a), implying that the jet is hydrodynamically unstable, but it is difficult to say to what extent the IPV maximum is directly associated with convection, since the convective region, signified by the diabatic heating and the WRF model rainfall, is stretched out and elongated from southwest to northeast for both systems, with the IPV maximum near 11N lying in the middle of this elongated region. But regardless of the source of the instability, both waves appear to be virtually identical with regard to their instability patterns.

Both waves exhibit barotropic instability, with the maximum value of the integrand in Eq. (8) being larger for the Florence wave. Interestingly, the location of the positive conversion is to the west of the Julia wave axis and to the east of the Florence wave axis. This pattern was characteristic of the two systems well into the storm stage. In both cases the positive region signifies eddy momentum flux down the mean momentum gradient. For the Julia wave the easterly wind maximum manages to migrate to the west of the wave axis, where the positive conversion results from the product of negative u' and negative v'. For the Florence wave, the easterly wind maximum remains to the north of the center of circulation, and the positive conversion occurs on the east side of the wave from the product of positive u' and positive v'. This difference in the energetics pattern is interesting but does not appear to be significant in explaining the different intensity outcomes for the two systems, particularly since the barotropic conversion is stronger for the Florence wave which yielded the weaker storm.

It is of particular significance for this study that the regions of positive barotropic conversion, positive baroclinic conversion, diabatic heating, and model rainfall are all superimposed for both systems. For Julia this superposition is to the west of the wave axis (Fig. 3), and for Florence it is primarily to the east of the wave axis (Fig. 4). This interesting pattern is driven by convection. The rising warm air in the convection triggers the positive baroclinic conversion [$\omega' T'$ in Eq. (9)], and the convective regions, of course, are regions of strong diabatic (condensational) heating and of rainfall. Further, Hsieh and Cook (2007)

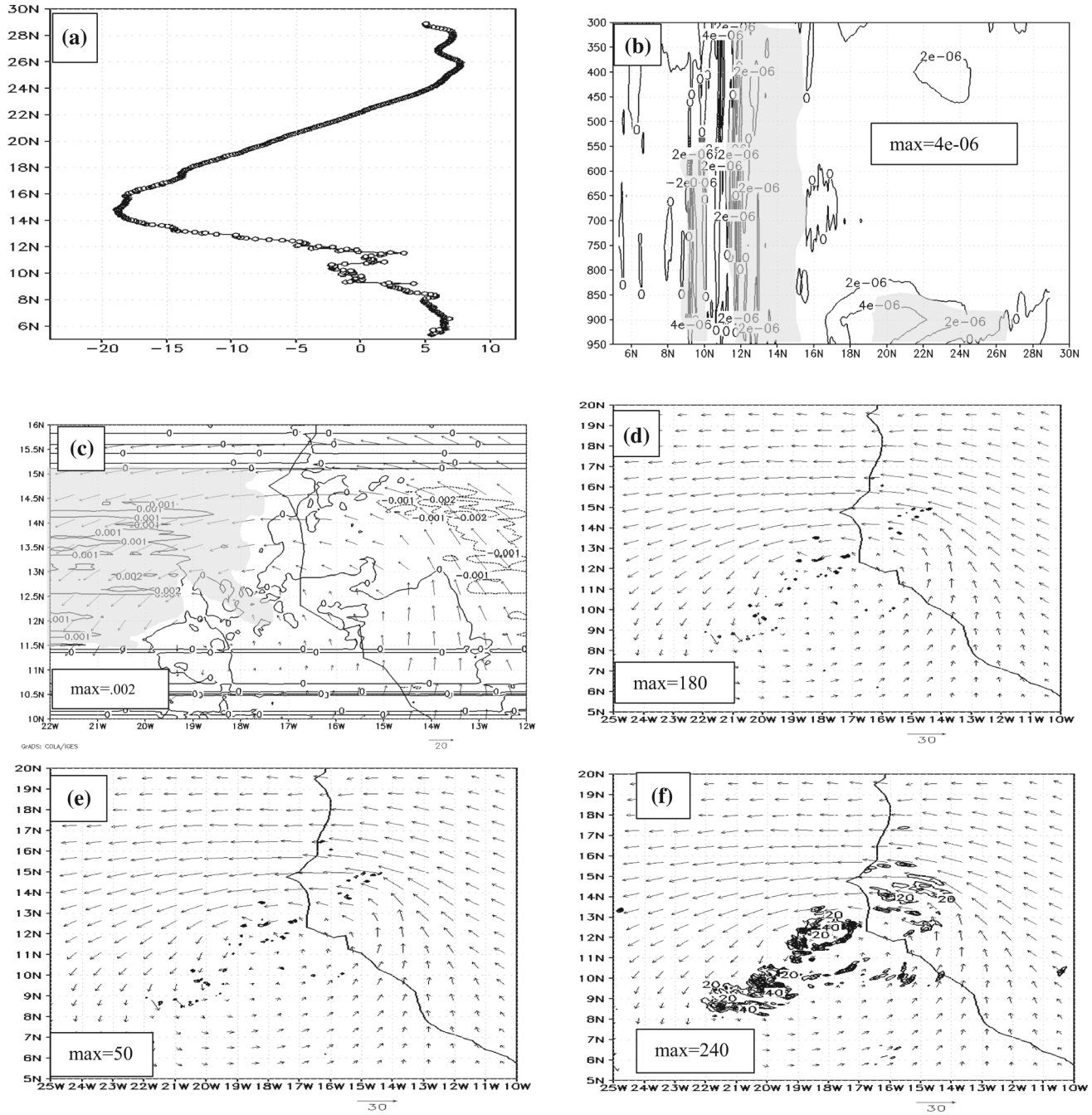

Fig. 3 **a** Profile of mean 650 hPa u-wind in m s^{-1}along 19W for the period 2100 UTC 11 September 2010 to 0300 UTC 12 September 2010, **b** cross section of mean isentropic potential vorticity, $-\varsigma_{a\theta}g\partial\theta\partial p^{-1}$, along 19W for the same period with interval 2e-06 $kg^{-1}m^2s^{-1}K$, with shading for regions of negative meridional IPV gradient, **c** integrand for term C_{k1} in Eq. (8), $-u'v'\partial u\partial y^{-1}$, with interval 0.001 W kg^{-1}(shading for positive regions), and wind vectors, both at 600 hPa at 0000 UTC 12 September 2010 (d) integrand for term C_{pk}in Eq. (9), $-\omega' T'$, with interval 20 Pa s^{-1} K, and wind vectors, both at 600 hPa at 0000 UTC 12 September 2010, **e** diabatic heating, $c_pT\theta^{-1}d\theta dt^{-1}$ with interval 10 m^2s^{-3}, and wind vectors, both at 600 hPa at 0000 UTC 12 September 2010 (f) WRF model rain for the period 2100 UTC 11 September 2010–0300 UTC 12 September 2010 with interval 20 mm, along with 600 hPa wind vectors at 0000 UTC 12 September 2010

found that significant barotropic instability was induced by deep convection on the southern flank of the AEJ. They state that in active waves there is usually an in-phase evolution of baroclinic and barotropic conversions in regions of active rainfall, as the barotropic instability induced by the convection enhances the baroclinic overturning through the resonance of these two instabilities. Thus, this study and the earlier one of Hsieh and Cook both

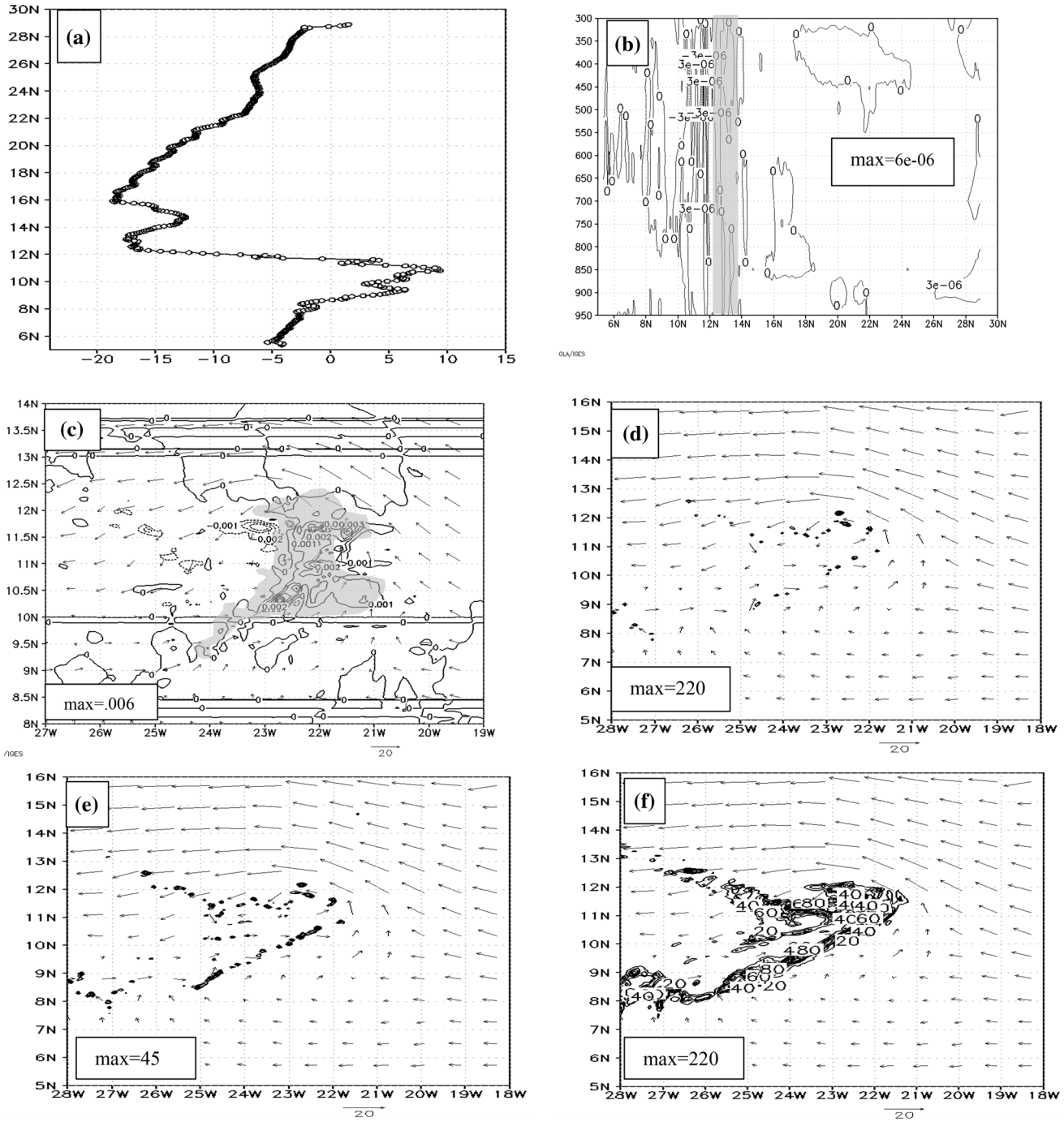

Fig. 4 **a** Profile of mean 650 hPa u-wind in m s^{-1}along 22W for the period 0900 UTC 03 August 2012–1500 UTC 03 August 2012, **b** cross section of mean isentropic potential vorticity, $-\varsigma_{a\theta}g\partial\ \theta\partial p^{-1}$, along 22W for the same period with interval 3e-06 $kg^{-1}m^2s^{-1}K$, with *shading* for regions of negative meridional IPV gradient, **c** integrand for term C_{k1} in Eq. (8), $-u'v'\partial u\partial y^{-1}$, with interval 0.001 W kg^{-1} (*shading* for positive regions), and wind vectors, both at 600 hPa at 1200 UTC 03 August 2012, **d** integrand for term C_{pk} in Eq. (9), $-\omega'T'$, with interval 20 Pa s^{-1} K, and wind vectors, both at 600 hPa at 1200 UTC 03 August 2012 (e) diabatic heating, $c_pT\theta^{-1}d\theta dt^{-1}$ with interval 5 m^2s^{-3}, and wind vectors, both at 600 hPa at 1200 UTC 03 August 2012 (f) WRF model rain for the period 0900 UTC 03 August 2012–1500 UTC 03 August 2012 with interval 20 mm, along with 600 hPa wind vectors at 1200 UTC 03 August 2012

stress the critical importance of convection in maintaining the energy of the waves, through diabatic heating which generates eddy available potential energy [$T'Q'$ in Eq. (11)] and through the resonance of barotropic and baroclinic conversions which generates the eddy kinetic energy. If anything disrupts the convection in a significant way this

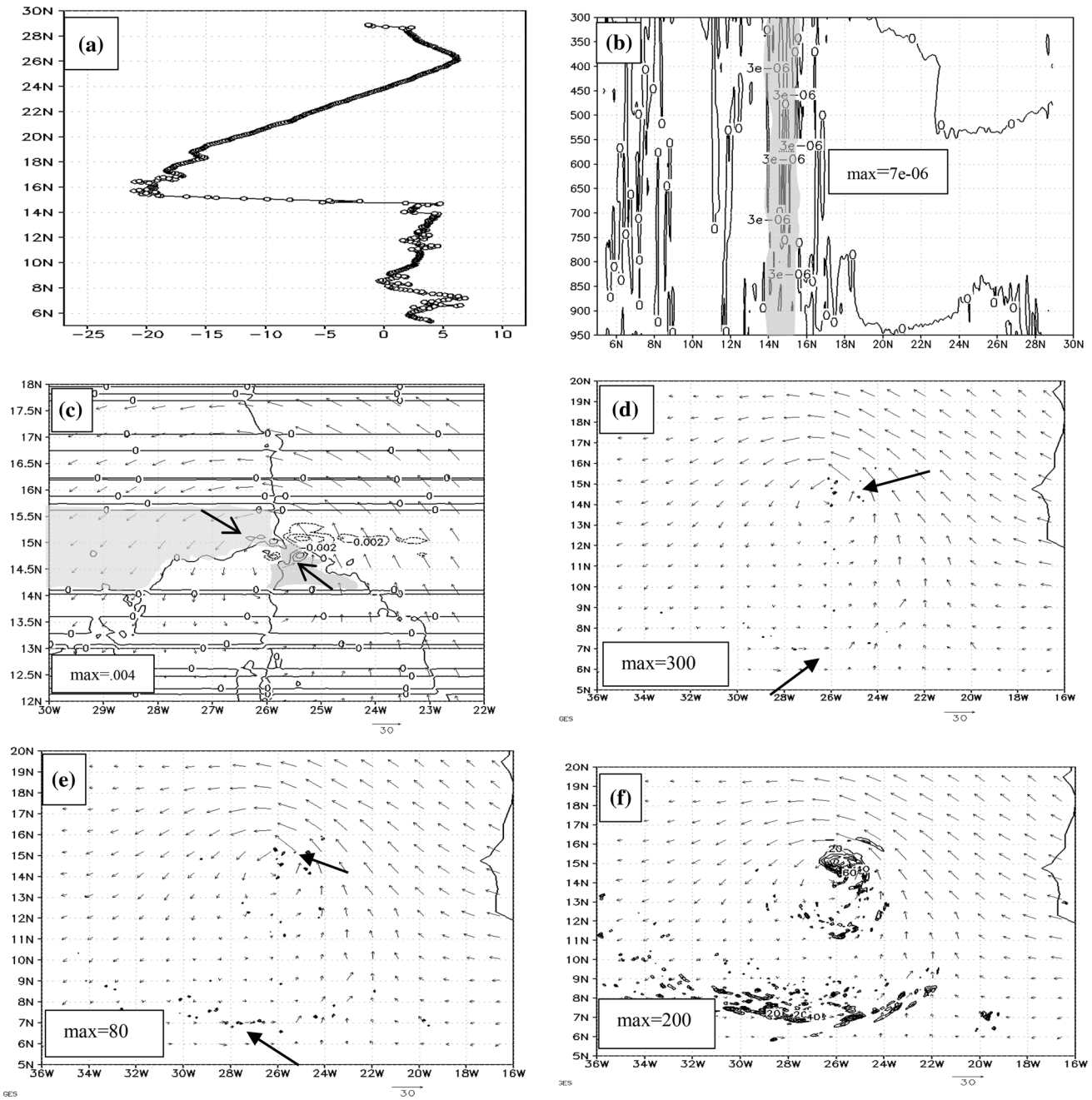

Fig. 5 **a** Profile of mean 650 hPa u-wind in m s^{-1}along 26W for the period 1500 UTC 13 September 2010 to 2100 UTC 13 September 2010, **b** cross section of mean isentropic potential vorticity, $-\varsigma_{a\theta}g\partial\ \theta\partial\ p^{-1}$, along 26W for the same period with interval 3e-06 $kg^{-1}m^2s^{-1}K$, with shading for regions of negative meridional IPV gradient (c) integrand for term C_{k1} in Eq. (8), $-u'v'\partial u\partial y^{-1}$, with interval 0.002 W kg^{-1}(*shading* for positive regions), and wind vectors, both at 600 hPa at1800 UTC 13 September 2010, **d** integrand for term C_{pk} in Eq. (9), $-\omega'T'$, with interval 50 Pa s^{-1} K, and wind vectors, both at 600 hPa at 1800 UTC 13 September 2010, **e** diabatic heating, $c_pT\theta^{-1}d\theta dt^{-1}$ with interval 10 m^2s^{-3}, and wind vectors, both at 600 hPa at 1800 UTC 13 September 2010, **f** WRF model rain for the period 1500 UTC 13 September 2010–2100 UTC 13 September 2010 with interval 20 mm, along with 600 hPa wind vectors at 1800 UTC 13 September 2010

pattern of energy production may fall like a house of cards, and the wave may weaken or disintegrate.

Significantly, Julia maintains this convectively driven energy production cycle into the storm stage (Fig. 5) but this cycle breaks down in Florence (Fig. 6). Julia continues to exhibit combined barotropic-baroclinic instability in the region of sign reversal in the meridional IPV gradient, indicated by shading. This instability continues to occur, as

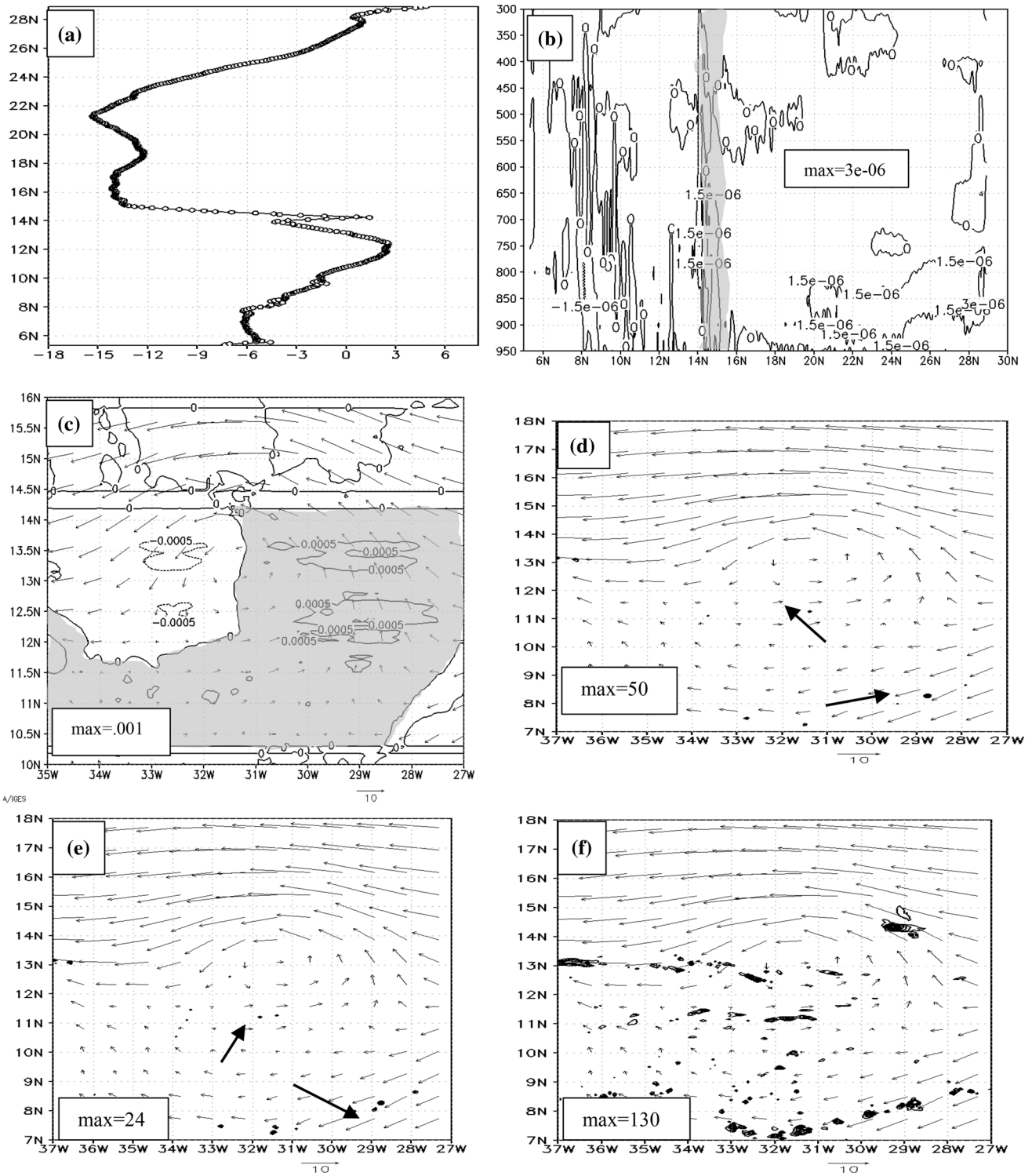

Fig. 6 **a** Profile of mean 650 hPa u-wind in m s^{-1}along 29W for the period 0900 UTC 05 August 2012–1500 UTC 05 August 2012, **b** cross section of mean isentropic potential vorticity, $-\varsigma_{a\theta}g\partial\ \theta\partial\ p^{-1}$, along 29W for the same period with interval 1.5e-06 $kg^{-1}m^2s^{-1}$ K, with shading for regions of negative meridional IPV gradient, **c** integrand for term C_{k1} in Eq. (8), $-u'v'\partial u\partial y^{-1}$, with interval 0.0005 W kg^{-1}(*shading* for positive regions), and wind vectors, both at 600 hPa at 1200 UTC 05 August 2012, **d** integrand for term C_{pk} in Eq. (9), $-\omega'T'$, with interval 5 Pa s^{-1} K, and wind vectors, both at 600 hPa at 1200 UTC 05 August 2012 (e) diabatic heating, $c_pT\theta^{-1}$ $d\theta dt^{-1}$ with interval 3 m^2s^{-3}, and wind vectors, both at 600 hPa at 1200 UTC 05 August 2012, **f** WRF model rain for the period 0900 UTC 05 August 2012–1500 UTC 05 August 2012 with interval 10 mm, along with 600 hPa wind vectors at 1200 UTC 05 August 2012

in Julia's wave stage, in a region of strong horizontal wind shear to the south of the AEJ (see panel a). The IPV maximum near 14.5N does appear to be directly associated with the convection located near the storm center, as signified by the region of diabatic heating near 15N, 25W (arrow in panel e) and the model rain (large circular region near 15N, 25W (see panel f). The regions of positive barotropic and baroclinic conversions, as well as the region of diabatic heating (indicated by small arrows in panels c, d, and e, respectively, in Fig. 5), are all smaller in geographic extent, but significantly larger in magnitude, than in Julia's wave stage (Fig. 3), indicating that Julia is still strengthening (barotropic conversion integrand, 0.002 to 0.004; baroclinic conversion integrand, 180–300; diabatic heating, 50–80). And these regions, along with the region of model rain, are all superimposed, maintaining the convectively driven energy production cycle.

The energetics patterns for Florence in the storm stage are shown in Fig. 6. Panel a and b are similar to those in Julia's storm stage in Fig. 5, with combined barotropic–baroclinic instability, implied by a region of sign reversal in the meridional IPV gradient (shaded region), lying within a region of strong horizontal wind shear to the south of the AEJ. Unlike Julia's storm stage, the IPV maximum near 14N is not associated with convection at that latitude as indicated by the diabatic heating and only remotely connected with convection at that latitude as indicated by the model rain. The region of positive barotropic conversion is much weaker than it was in Florence's wave stage (reduced from 0.006 to 0.001), and this region is not superimposed on the region of positive baroclinic conversion, which is much smaller and much weaker than in Florence's wave stage (reduced from 220 to 50) and shifted to the south of the region of positive barotropic conversion. The very much weakened baroclinic conversion indicates a much reduced lifting of warm air in convection as compared to the wave stage, and this is consistent with the smaller and weaker regions of diabatic heating (reduced from 45 to 24). Florence has lost its convectively driven energy production cycle, as the parameters directly linked to convection (baroclinic conversion, diabatic heating, model rain) have all been weakened and displaced well to the south of the storm's circulation center and out of phase with the positive barotropic conversion. The model rain penetrates the farthest northward, but no rain is seen north of an east–west line running through the storm's center along 13N. In Julia; by contrast, the diabatic heating (Fig. 5e), the model rain (Fig. 5f) and the baroclinic conversion (Fig. 5d) all have significant placements in, and slightly to the north of, the storm center, as well as further to the south along the ITCZ. The locations of these parameters in the vicinity of the storm center are also in phase with the positive barotropic conversion, and the convectively driven energy production cycle is maintained.

Fig. 7 **a** Dew point temperature with interval 3 C at 850 hPa for 1200 UTC 5 August 2012. **b** Cross section of relative humidity with interval of 10 % along longitude 29W in panel (**a**) for 1200 UTC 5 August 2012. **c** Temperature (*solid*) and dew point temperature (*dashed*) profiles in C at location 20N, 30W in panel (**a**) for 1200 UTC 5 August 2012

In summary, by the storm stages depicted in Figs. 5 and 6, Florence is a weaker storm than Julia, and is destined to become even weaker, as indicated by the maximum values of key energetics parameters: IPV, 7e-06 (J) and 3e-06 (F); barotropic conversion integrand, 0.004 (J) and 0.001 (F); baroclinic conversion integrand, 300 (J) and 50 (F); diabatic heating, 80 (J) and 24 (F); model rain, 200 (J) and 130 (F). Most importantly, the convection in Florence has weakened significantly and has been shifted southward away from the storm's center, as the convectively driven energy production cycle described in this section is lost. Such changes have not been observed in Julia. The next section will offer an explanation of why the convection evolves so differently in the two storms, with the resultant radically different storm intensities. At the core of the explanation is the role of the SAL.

6 The disparate impacts of the SAL on the convection in Florence and Julia

This section will explore the extent to which the SAL disrupted the convection in Florence, but not in Julia. The emphasis will be on three primary impacts of the SAL in suppressing tropical cyclone activity that were developed by Dunion and Velden (2004): evaporative effects of the dry air, stabilizing effects of an enhanced trade wind inversion, increased vertical wind shear due to the presence of the mid-level AEJ. Figures 7 and 8 will address these impacts for Florence, while Figs. 9 and 10 will do the same for Julia.

Figure 7a, b depicts the patterns of dry air in the environment of Tropical Storm Florence at 1200 UTC 5 August 2012 (same time as Fig. 6). Figure 7a shows 850 hPa dew point temperature for the region extending from West Africa into the central Atlantic. Florence's center is near the maximum in dew point temperature around 15N and 28W. What is most striking about this figure is that dry air extends almost continuously over a huge area from West Africa westward across the Atlantic to approximately 40W, with the core of the dry air possessing negative dew point temperatures. The dry air curls around the circulation of Florence on the western and southern sides. The gradient in

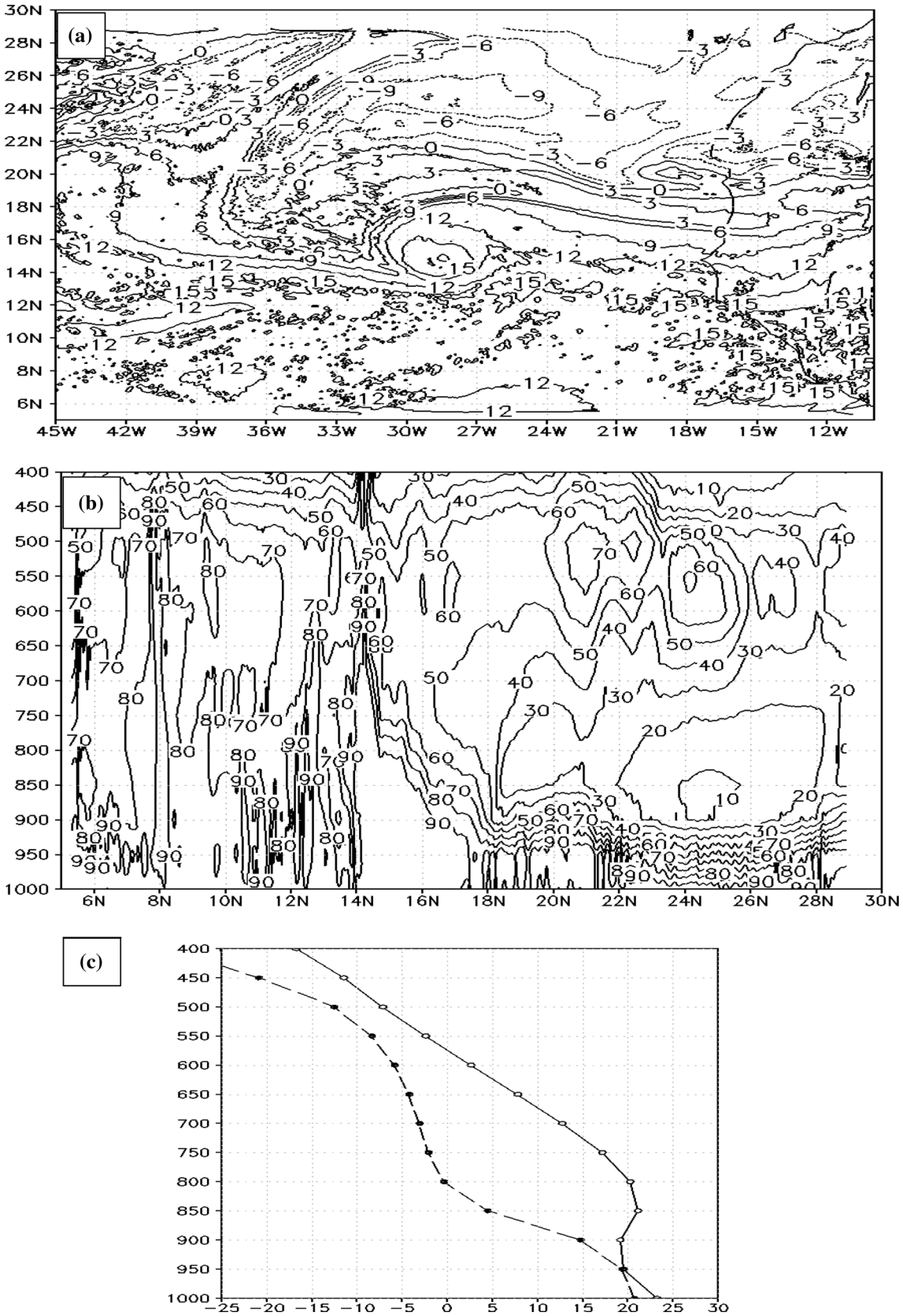
(a)
30N
28N
26N
24N
22N
20N
18N
16N
14N
12N
10N
8N
6N
45W
42W
39W
36W
33W
30W
27W
24W
21W
18W
15W
12W
(b)
400
450
500
550
600
650
700
750
800
850
900
950
1000
6N
8N
10N
12N
14N
16N
18N
20N
22N
24N
26N
28N
30N
(c)
400
450
500
550
600
650
700
750
800
850
900
950
1000
−25 −20 −15 −10 −5 0 5 10 15 20 25 30

dew point temperature is very tight and front-like to the north of Florence, where the dew point drops from 12 to 0 °C across only two degrees of latitude. The dry air is depicted from a different perspective in the north–south cross section of relative humidity along 29W in Fig. 7b. This section passes through the moist region of Florence near 15N and extends into the very dry air further to the north where dew point temperatures in Fig. 7a drop to −9 °C. A very large and compact region of dry air, with relative humidity values dropping to 10 %, exists to the north of Florence's moist region from 18 to 29N, and from 900 to 700 hPa in the vertical.

Figure 7c explores the strength of the trade wind inversion through vertical profiles of temperature and dew point temperature at 20N, 30W in the very dry air to the north of Florence's 850 hPa center. A moist marine layer extends from 1000 to 950 hPa, where saturation signifies the formation of trade wind cumulus. Above this, a sharp inversion extends up to 850 hPa, with pronounced warming and drying. The top of this inversion represents the base of the SAL which extends upward as a warm and dry layer to around 600 hPa. The maximum dew point depression in this layer is an impressive 22 °C at 800 hPa. The presence of the SAL has enhanced the normal trade wind inversion in this region.

Figure 8 examines the mid-level AEJ associated with the SAL, along with its impact on the vertical wind shear in the vicinity of Tropical Storm Florence at 1200 UTC 5 August 2012 (same as Fig. 7). Figure 8a shows wind vectors and isotachs at 600 hPa. An expansive wind maximum representing the AEJ extends in the latitude belt 15–24N from West Africa across the Atlantic to 45W, with speeds to 15 m s^{-1}(30 knots). To the north of the wind maximum a nearly uninterrupted anticyclone stretches across the Atlantic with wind speeds below 5 m s^{-1}. The strong easterly flow at 600 hPa, with weaker winds above and below, produces pronounced westerly shear above 600 hPa (Fig. 8b) and pronounced easterly shear below 600 hPa (Fig. 8c). This places Tropical Storm Florence (600 hPa center indicated by an "X") in, or very close to, a highly sheared environment, with 20 knots of westerly shear above and just to the north of the center and 20 knots of easterly shear below and just to the north of the center. The expansive nature of the 600 AEJ produces correspondingly expansive regions of vertical wind shear.

The front-like quality to the dew point temperature gradient, the location of the warm, dry air primarily in the layer 850–600 hPa, and the strong mid-level easterly jet (AEJ) associated with the strong temperature and moisture gradients are all signature indicators of a "Saharan air outbreak" over the northern equatorial Atlantic as first described by Carlson and Prospero (1972). The presence of this Saharan air is further substantiated in the National Hurricane Center's Tropical Cyclone Report on Tropical Storm Florence (Cangialosi, 2012). The expansive nature of the regions of dry air, of the anticyclone, and of the AEJ, all of which extend essentially unbroken from West Africa into the central Atlantic, are strongly suggestive that Florence developed from a wave with a periodicity of 6–9 days and a wavelength of about 6000 km instead of the more typical AEW with a periodicity of 3–5 days and a wavelength of 2500–3000 km. Such atypical waves have been described by Diedhiou et al. (1998) and Karyampudi and Carlson (1988), and they have been described as waves associated with very large anticyclonic circulations north or the jet, as seen in the Florence case.

Fig. 8 **a** Wind vectors and isotachs with an interval of 5 m s^{-1} at 600 hPa for 1200 UTC 5 August 2012, **b** wind shear vectors and isotachs with an interval of 10 m s^{-1} for the layer 350 hPa to 600 hPa (350–600 hPa vector), **c** wind shear vectors and isotachs with an interval of 10 m s^{-1} for the layer 600 hPa to 850 hPa (600–850 hPa vector). Both **b** and **c** are for the same time as **a**. *X marks* 600 hPa center ▶

What is most important for our purposes is that the evaporative effects of the huge region of dry air just to the north of Florence, the stabilizing effects of the enhanced trade wind inversion, and the strong vertical wind shear in the storm's environment would all have a very strong detrimental effect on the formation and maintenance of organized deep convection. Figures 9 and 10 will seek to determine to what extent Julia may have experienced detrimental impacts from the SAL.

Figure 9a, b depicts the patterns of dry air in the environment of Julia when it was still a tropical storm at 1800 UTC 13 September 2010 (same as Fig. 5). Figure 9a shows the 850-hPa dew point temperature for the region from West Africa into the central Atlantic. Julia's 850 hPa center is near the maximum in dew point temperature around 15N and 25W. Unlike the dew point temperature pattern for Florence in Fig. 7a, dry air does not extend continuously across the area from West Africa into the central Atlantic but is present in two distinct regions, one over West Africa and another to the north and west of Julia. The air is not nearly as dry as with Florence and is essentially free of negative dew points. The dry air does curl around the center of Julia to the west and south (indicated by three arrows), but Julia retains a large core of moist air. The gradient in dew point temperature to the north and west of Julia is not front-like as with Florence. The dry air is depicted from a different perspective in the north–south cross section of relative humidity along 26W in Fig. 9b. This section passes through the moist region of Julia near 15N and extends into the dry air to the north. This dry region (indicated by an arrow) is not nearly as large and compact as in the Florence cross-section

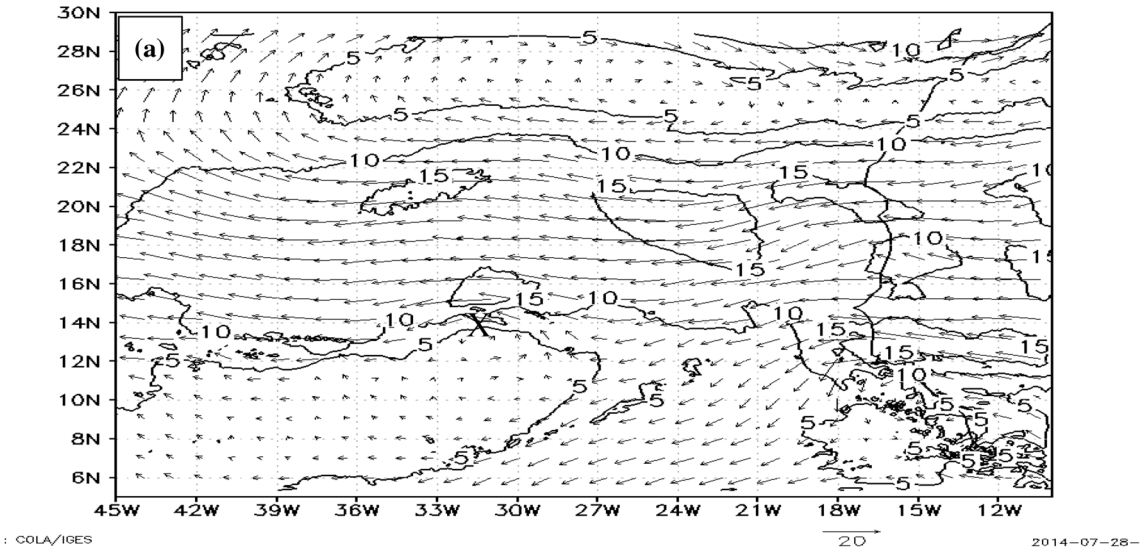
(a)
30N
28N
26N
24N
22N
20N
18N
16N
14N
12N
10N
8N
6N
45W 42W 39W 36W 33W 30W 27W 24W 21W 18W 15W 12W
20
2014-07-28-

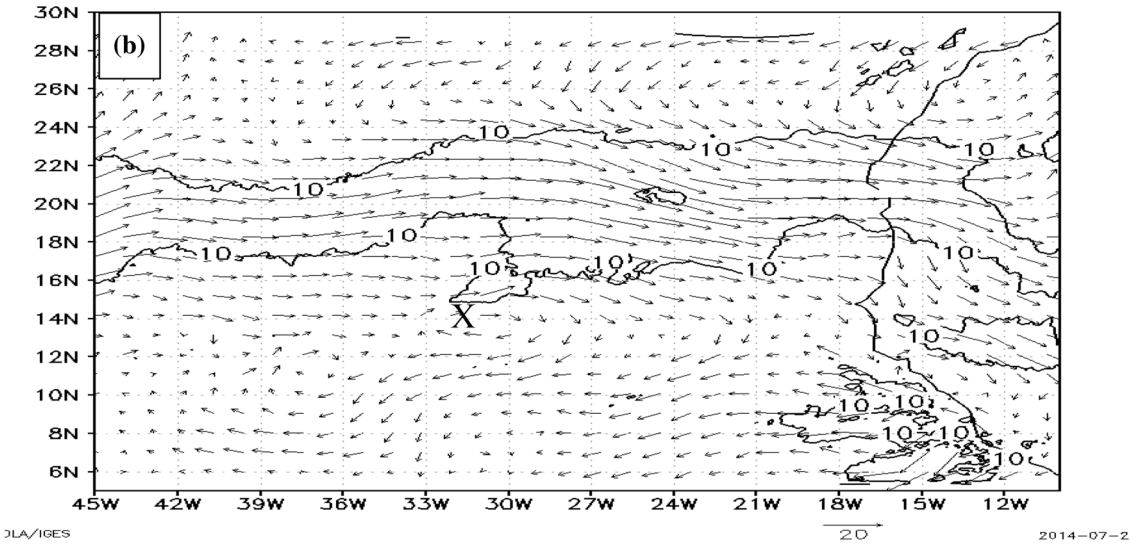
(b)
30N
28N
26N
24N
22N
20N
18N
16N
14N
12N
10N
8N
6N
45W 42W 39W 36W 33W 30W 27W 24W 21W 18W 15W 12W
20
2014-07-2

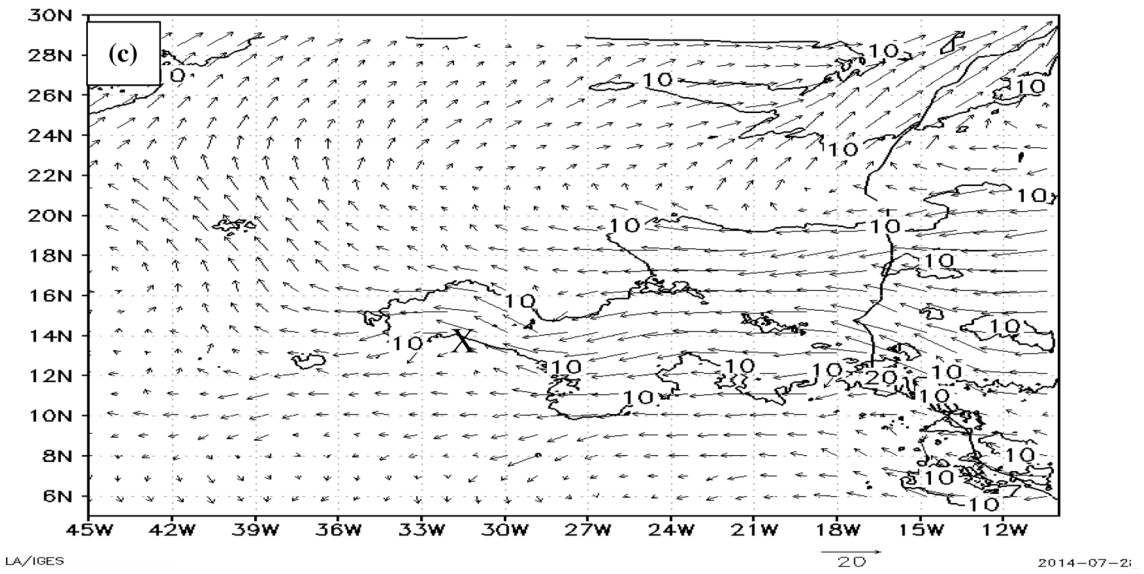
(c)
30N
28N
26N
24N
22N
20N
18N
16N
14N
12N
10N
8N
6N
45W 42W 39W 36W 33W 30W 27W 24W 21W 18W 15W 12W
20
2014-07-2

(Fig. 7b) and is more elevated with minimum relative humidity values of 20 % as opposed to 10 % for Florence. The strip of dry air curling around Julia on the south side is seen near 10N (indicated by an arrow). Although dryer than the air in Julia's core, the minimum relative humidities are still in the 40–60 % range.

Figure 9c shows vertical profiles of temperature and dew point temperature at 23N, 30W in the dry air to the northwest of Julia's center. A moist marine layer is seen as with Florence (Fig. 7c) but there is no inversion above that layer. Without an inversion it is difficult to define the base of an elevated SAL which is typically found at the top of the inversion. Likewise, there are no distinguishing features to define the top of a SAL. Dry air exists aloft but the maximum dew point depression is about 15 C at 800 hPa, as compared to 22 C for the Florence case. There is no evidence that a trade wind inversion has been enhanced by a SAL in the Julia case.

Figure 10 explores the mid-level easterly jet (AEJ) at 600 hPa and the pattern of vertical wind shear above and below that jet for Tropical Storm Julia at 1800 UTC 13 September 2010 (same as Fig. 9). The center of Julia's circulation is indicated with an "X." There are salient differences between this figure and the one for Florence: there is no expansive AEJ extending across the entire map area, but more of a broken pattern with wind maxes over West Africa, one directly associated with Julia, and a third one near 45W (Fig. 10a); there is no expansive and uninterrupted anticyclone extending across the Atlantic to the north of the wind maxima; there is no elongated region of westerly shear above and to the north of Julia's 600 hPa center (Fig. 10b); there is no elongated region of easterly shear below and to the north of Julia's 600 hPa center (Fig. 10c). Compared to Florence, Julia is in a relatively low-shear environment.

The difficulty in locating the SAL in the vertical profiles of temperature and dew point temperature (Fig. 9c) and the lack of a front-like gradient in the dew point temperature map at 850 hPa (Fig. 9a) suggest the absence of a classic "Saharan air outbreak" in the Julia case. Further, the Julia wave appears to be the more typical AEW with a wavelength of 2500–3000 km, rather than the 6000-km wavelength wave likely associated with Florence. The evidence for this is the absence of an expansive region of dry air and of a broad anticyclone to the north as was seen in the Florence case. Most importantly, the lack of the evaporative effects of a huge and very dry air mass to the north, of the stabilizing effects of a SAL-enhanced trade wind inversion, and of strong vertical wind shear, would all indicate that the organized deep convection in Julia would have been free of significant inhibition.

The disparity in the inhibiting effect of the SAL on the convection and rainfall in Florence and Julia is emphatically illustrated in Figs. 11 and 12. Figure 11a shows the WRF model cloud water mixing ratio at 700 hPa for Florence at 0000 UTC 5 August 2012 at the time of maximum intensity of the tropical storm, while Fig. 11b shows the same parameter at 600 hPa for Julia at 1800 UTC 15 September 2010 close to the time of maximum intensity of the major hurricane. The difference in the distribution of cloud water is striking, as the dry air to the north of Florence has completely eliminated any cloud water in the northeastern semicircle. In contrast, the less hostile environment in Julia has allowed an eye wall feature to form in the cloud water, as well as extensive condensation to the northeast of the center.

Figure 12 shows the total accumulated WRF model precipitation for the full 5-day forecast for Florence (Fig. 12a) and for Julia (Fig. 12b). There is no precipitation whatsoever to the north of approximately 14N in the Florence case due to the hostile effects of the SAL. The small strip of precipitation extending northwestward from about 12N, 24W represents the track of Florence. In contrast, the wide strip of precipitation extending northwestward from about 12N, 21W represents the track of Julia, a storm that was able to travel northward due to the lack of a strong inhibiting SAL.

7 Summary and conclusions

Hurricane Julia (2010) and Tropical Storm Florence (2012) both developed from AEWs over the eastern Atlantic, with Julia becoming a major hurricane and Florence weakening to a wave after becoming a tropical storm. This paper's goal was to explain these different outcomes using WRF model 5-day simulations as the basis for a complete energetics study of each storm. NWP models can simulate the wave dynamics and energetics with a time and space resolution that is not possible with existing observational systems and re-analysis. The paper sought to determine if there were significant differences in the structures and energetics of the two precursor AEWs that may have contributed to the very different tropical cyclones that they produced and, very importantly, to assess the role of the SAL in explaining their different intensities. Determination of the role of the SAL in Atlantic cyclogenesis is a major goal of NASA's Hurricane and Severe Storm Sentinel (HS3) Project whose field phase was conducted in the Atlantic during the summers of 2012-2014. In this paper the role of the SAL is assessed quantitatively based on a complete energetics study. In this sense the study goes beyond previous studies that have been based on purely qualitative assessments of the SAL.

The research showed that the different outcomes for Julia and Florence could be explained by significant

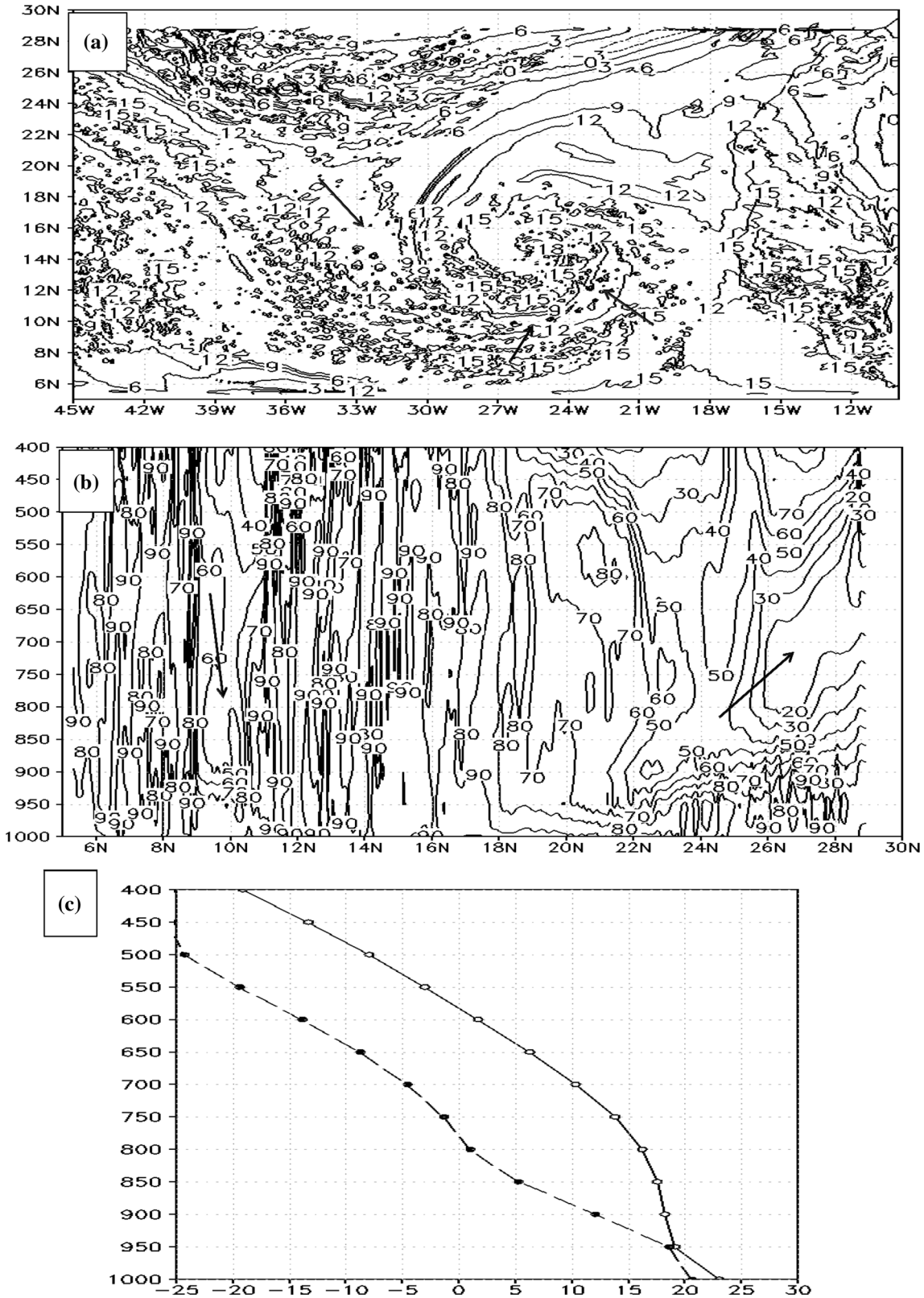

Fig. 9 **a** Dew point temperature with interval 3 °C at 850 hPa for 1800 UTC 13 September 2010, **b** cross section of relative humidity with interval of 10 % along longitude 26W in panel (**a**) for 1800 UTC 13 September 2010. **c** Temperature (*solid*) and dew point temperature (*dashed*) profiles in C at location 23N, 30W in panel (**a**) for 1800 UTC 13 September 2010

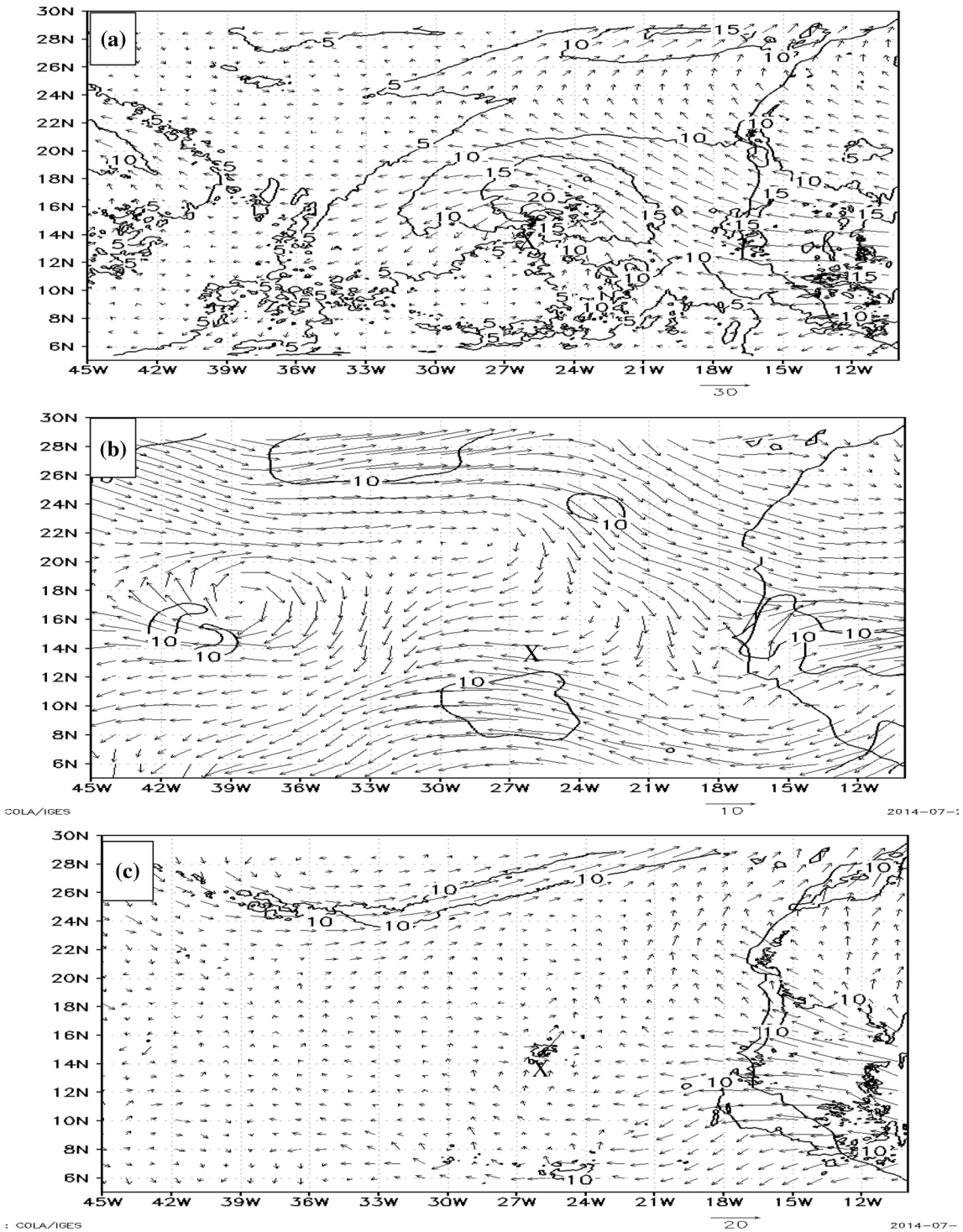

Fig. 10 **a** Wind vectors and isotachs with an interval of 5 m s^{-1} at 600 hPa for 1800 UTC 13 September 2010, **b** wind shear vectors and isotachs with an interval of 10 m s^{-1} for the layer 350–600 hPa (350–600 hPa vector), **c** wind shear vectors and isotachs with an interval of 10 m s^{-1} for the layer 600–850 hPa (600–850 hPa vector). Both **b** and **c** are for the same time as **a**. *X marks* 600 hPa center

differences in their energetics patterns that emerged in their storm stages due to differences in the impact of the SAL. There were no significant differences in the energetics of the two systems in their wave and depression stages. In the wave and depression stages Florence was actually more energetic than Julia. In those stages the eddy kinetic energy in both systems was maintained by barotropic and baroclinic conversions, with the latter being dominant. The

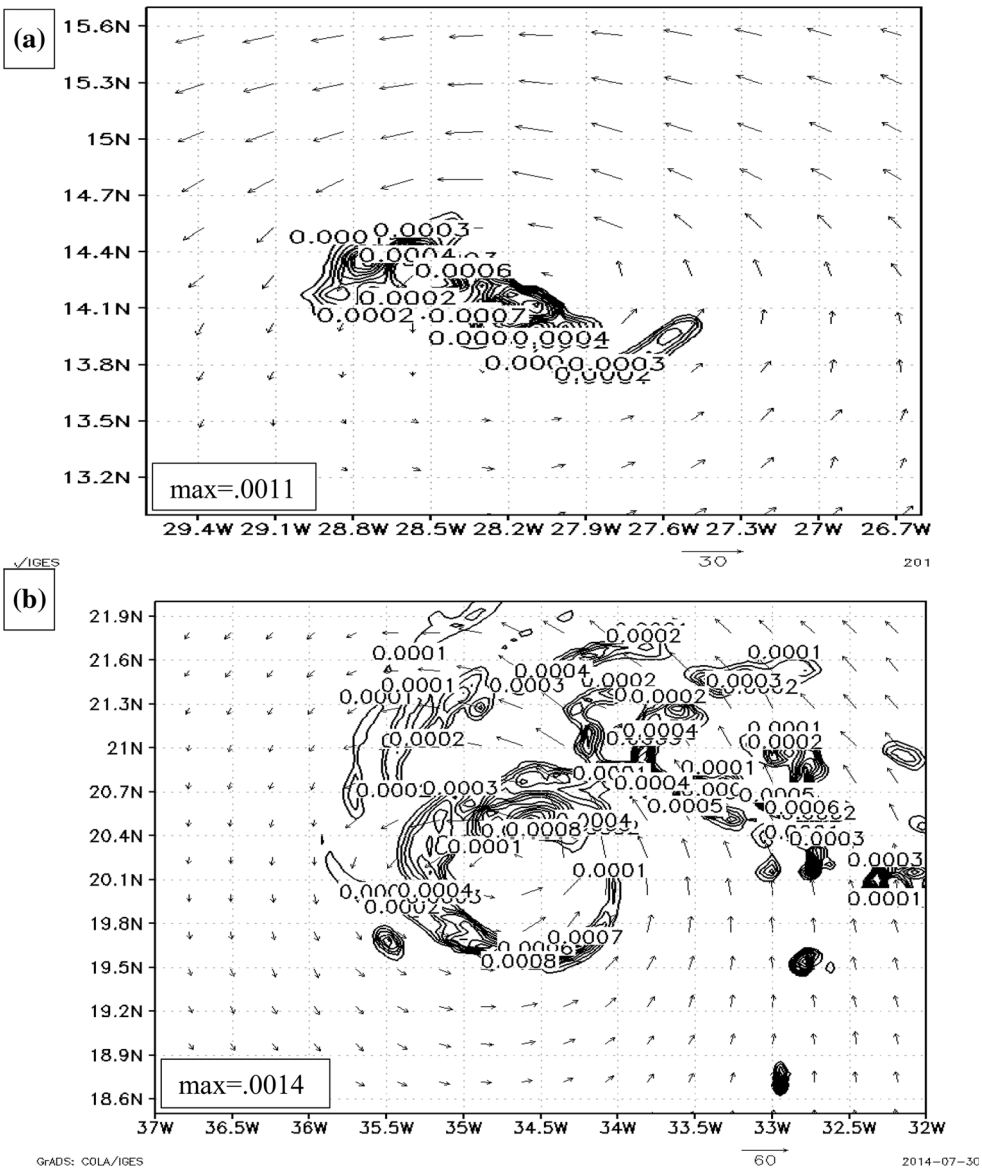

Fig. 11 **a** Cloud water mixing ratio with interval of 0.0001 kg kg^{-1} and wind vectors both at 700 hPa in Tropical Storm Florence at 0000 UTC 5 August 2012, **b** cloud water mixing ratio with interval of 0.0001 kg kg^{-1} and wind vectors both at 600 hPa in Major Hurricane Julia at 1800 UTC 15 September 2010

eddy available potential energy was maintained by both the conversion of zonal to eddy available potential energy and by the generation of eddy available potential energy by diabatic heating in convection, with the latter being dominant. Significantly, for both systems the regions of positive barotropic and baroclinic conversion, as well as the regions of diabatic heating and model rainfall, were superimposed during the wave and depression stages, a pattern that is driven by convection. Hsieh and Cook (2007) found that convection induces barotropic instability which then enhances the baroclinic overturning through a resonance of the two instabilities. The baroclinic conversion is also directly maintained by the rising warm air in the convection, and the convection, of course, produces condensational heating and rainfall. The diabatic heating in the convection generates the eddy available potential energy which, along with the eddy kinetic energy, defines the total eddy energy of the system.

This study showed that Florence lost this convectively driven energy production cycle in the storm stage and began to weaken, while Julia maintained the cycle and became a major hurricane. As Florence's convection weakened, the convectively driven fields of baroclinic conversion, diabatic heating, and model rain all became weaker and were displaced well to the south of the storm's circulation center and out of phase with the positive barotropic conversion, eliminating the resonance between the barotropic and baroclinic conversions. In Julia these parameters all remained near the storm's center and in phase with the positive barotropic conversion.

The major finding of the study was that the disruption of the convection in Florence, which led to its demise, was

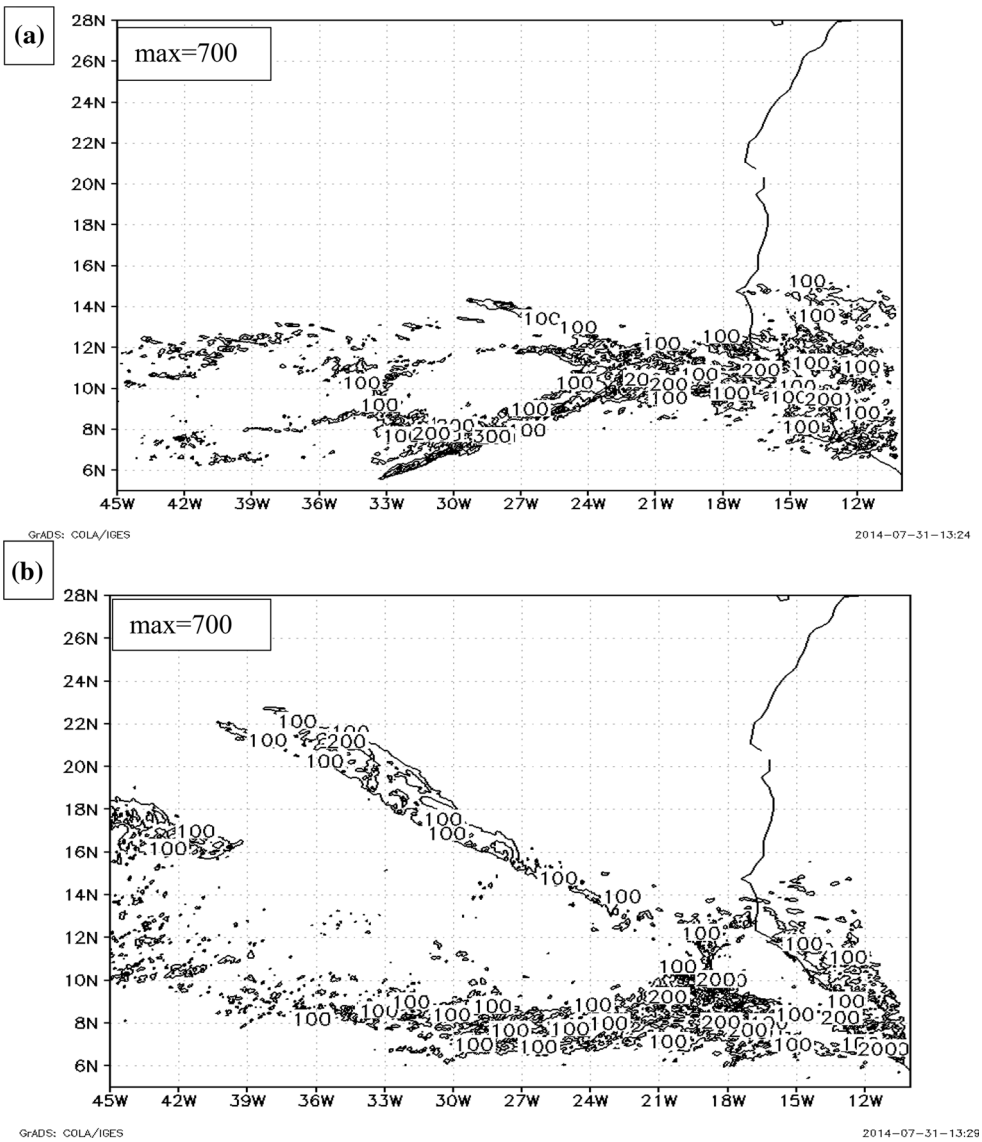

Fig. 12 **a** Accumulated WRF model precipitation with interval of 100 mm for the full 5-day forecast of Florence, extending from 1200 UTC 2 August 2012 to 1200 UTC 7 August 2012, **b** accumulated WRF model precipitation with interval of 100 mm for the full 5-day forecast of Julia, extending from 1200 UTC 11 September 2010 to 1200 UTC 16 September 2010

due to a pronounced SAL that lay to the north of the storm. Evidence for the presence of the SAL included the front-like quality to the dew point temperature gradient, the location of the warm, dry air in the layer 850–600 hPa, and a strong mid-level easterly jet to the south of a well-defined anticyclone, all of which are classic signatures of a Saharan air outbreak over the northern equatorial Atlantic, as first described by Carlson and Prospero (1972). The evaporative effects of an expansive region of dry air just to the north of Florence, the stabilizing effects of an enhanced trade wind inversion, and strong vertical wind shear in the storm's environment, all due to the presence of the SAL, had a detrimental effect on the formation and maintenance of organized deep convection.

By contrast, in the Julia case, the difficulty in locating the SAL in the vertical profiles of temperature and dew point temperature and the lack of a front-like gradient in the dew point temperature map at 850 hPa indicated the lack of a classic Saharan air outbreak to the north of the storm. Unlike in Florence, the convection in Julia was not inhibited, due to the lack of the drying, stabilizing, and vertical shearing effects of a well-formed SAL, and Julia was able to develop into a major hurricane by the convectively driven energy production cycle described above.

One final distinction between the Florence and Julia cases deserves to be mentioned. The expansive nature of the regions of dry air, of the anticyclone, and of the AEJ, all of which extended unbroken from West Africa into the central Atlantic, are strongly suggestive that Florence developed from a wave with a periodicity of 6–9 days and a wavelength of about 6000 km. By contrast, the absence of an expansive region of dry air and of a broad anticyclone

to the north of Julia suggests that Julia developed from the more typical AEW with a periodicity of 3–5 days and a wavelength of 2500–3000 km. Further research is needed to determine if storms that develop from the 6–9 day waves are more vulnerable to the detrimental effects of the SAL than those developing from the 3–5 day waves.

Acknowledgments This research was supported by National Aeronautics and Space Administration (NASA) Grant NNX12AJ77G.

Appendix: Energetics equations

$$K_{\mathrm{Z}} = \int_{p1}^{p2} \frac{\overline{[u]^2+[v]^2}}{2g}\mathrm{d}p \tag{3}$$

$$A_{\mathrm{Z}} = \int_{p1}^{p2} \frac{\overline{[T]^{*2}}}{2\overline{\sigma}}\mathrm{d}p \tag{4}$$

$$C_{\mathrm{Z}} = -\int_{p1}^{p2} \frac{R}{p}\overline{[\omega]^*[T]^*}\frac{\mathrm{d}p}{g} \tag{5}$$

$$K_{\mathrm{E}} = \int_{p1}^{p2} \frac{\overline{[u'^2+v'^2]}}{2g}\mathrm{d}p \tag{6}$$

$$A_{\mathrm{E}} = \int_{p1}^{p2} \frac{\overline{[T'^2]}}{2\overline{\sigma}}\mathrm{d}p \tag{7}$$

$$\begin{aligned} \mathrm{C_k} &= \mathrm{C_{k1}} + \mathrm{C_{k2}} + \mathrm{C_{k3}} + \mathrm{C_{k4}} \\ &= -\int_{p1}^{p2} \overline{[u'v']\frac{\partial[u]}{\partial y}}\frac{\mathrm{d}p}{g} - \int_{p1}^{p2} \overline{[u'\omega']\frac{\partial[u]}{\partial p}}\frac{\mathrm{d}p}{g} \\ &\quad -\int_{p1}^{p2} \overline{[v'^2]\frac{\partial[v]}{\partial y}}\frac{\mathrm{d}p}{g} - \int_{p1}^{p1} \overline{[v'\omega']\frac{\partial[v]}{\partial p}}\frac{\mathrm{d}p}{g} \end{aligned} \tag{8}$$

$$C_{\mathrm{pk}} = -\int_{p1}^{p2} \frac{R}{p}\overline{[\omega'T']}\frac{\mathrm{d}p}{g} \tag{9}$$

$$\begin{aligned} \mathrm{C_A} &= \mathrm{C_{A1}} + \mathrm{C_{A2}} \\ &= -\int_{p1}^{p2} \frac{\overline{[v'T']}}{\overline{\sigma}}\frac{\partial[T]}{\partial y}\mathrm{d}p - \int_{p1}^{p2} \frac{\overline{[\omega'T']}}{\overline{\sigma}}\frac{\partial[T]^*}{\partial p}\mathrm{d}p \end{aligned} \tag{10}$$

$$G_{\mathrm{E}} = \int_{p1}^{p2} \frac{\overline{[T'Q']}}{\overline{\sigma}c_p}\mathrm{d}p \tag{11}$$

$$D_{\mathrm{E}} = -\int_{p1}^{p2} \overline{\left[u'F'_x + v'F'_y\right]}\frac{\mathrm{d}p}{g} \tag{12}$$

$$\begin{aligned} K_{\mathrm{EB}} &= \frac{1}{L_x}\int_{p1}^{p2}\left[\left(\overline{\frac{u(u'^2+v'^2)}{2g}}\right)_{x1} - \left(\overline{\frac{u(u'^2+v'^2)}{2g}}\right)_{x2}\right]\mathrm{d}p \\ &\quad + \frac{1}{L_y}\int_{p1}^{p2}\left(\left[\overline{\frac{v(u'^2+v'^2)}{2g}}\right]_{y1} - \left[\overline{\frac{v(u'^2+v'^2]}{2g}}\right]_{y2}\right)\mathrm{d}p \\ &\quad + \left(\left[\overline{\frac{\omega(u'^2+v'^2)}{2g}}\right]_{p1} - \left[\overline{\frac{\omega(u'^2+v'^2)}{2g}}\right]_{p2}\right) \end{aligned} \tag{13}$$

$$\begin{aligned} \Phi_{\mathrm{EB}} &= \frac{1}{L_x}\int_{p1}^{p2}\left(\left(\overline{u'\phi'}\right)_{x1} - \left(\overline{u'\phi'}\right)_{x2}\right)\frac{\mathrm{d}p}{g} \\ &\quad + \frac{1}{L_y}\int_{p1}^{p2}\left([v'\phi']_{y1} - [v'\phi']_{y2}\right)\frac{\mathrm{d}p}{g} \\ &\quad + \frac{1}{g}\left(\overline{[\phi'\omega']}_{p1} - \overline{[\phi'\omega']}_{p2}\right) \end{aligned} \tag{14}$$

$$\begin{aligned} A_{\mathrm{EB}} &= \frac{1}{L_x}\int_{p1}^{p2}\left(\left(\overline{\frac{uT'^2}{2\bar{\sigma}}}\right)_{x1} - \left(\overline{\frac{uT'^2}{2\bar{\sigma}}}\right)_{x2}\right)\mathrm{d}p \\ &\quad + \frac{1}{L_y}\int_{p1}^{p2}\left(\left(\overline{\frac{[vT'^2]}{2\bar{\sigma}}}\right)_{y1} - \left(\overline{\frac{[vT'^2]}{2\bar{\sigma}}}\right)_{y2}\right)\mathrm{d}p \\ &\quad + \left(\left(\overline{\frac{[\omega T'^2]}{2\bar{\sigma}}}\right)_{p1} - \left(\overline{\frac{[\omega T'^2]}{2\bar{\sigma}}}\right)_{p2}\right) \end{aligned} \tag{15}$$

[()] represents a zonal mean and $\overline{[()]}$ represents a meridional mean of the zonal mean. Primes indicate deviations from the zonal mean, and asterisks indicate deviations from the area mean. The relationships are $() = [()] + ()'$ and $[()] = \overline{[()]} + ()^*$. Vaiables not mentioned in the text: K_Z is zonal kinetic energy, A_Z is zonal available potential energy, C_Z represents conversions between the two.

Following are the definitions of variables:

- u Zonal wind component, positive to the east
- v Meridional wind component, positive o the north
- ω Vertical pressure velocity
- T Temperature
- p Pressure
- F_x Friction in the zonal direction
- F_y Friction in the meridional direction
- Q Diabatic heating

ϕ Geopotential
$\overline{\sigma}$ Mean static stability ($gc_p^{-1}\ \overline{[T]}$ - $gpR^{-1}\ \partial\overline{[T]}\ \partial\ p^{-1}$)
c_p specific heat at constant pressure
R Specific gas constant for dry air
g Gravitational acceleration
x Zonal coordinate, positive to east
y Meridional coordinate, positive to north
L_x Zonal distance for the domain
L_y Meridional distance for the domain

References

Avila LA, Pasch R, Jing J (2000) Atlantic tropical systems of 1996 and 1997: years of contrast. Mon Wea Rev 128:3695–3706

Burpee RW (1972) The origin and structure of easterly waves in the lower troposphere of North Africa. J Atmos Sci 29:77–90

Cangialosi JP (2012) Tropical Cyclone Report, Tropical Storm Florence (AL062012), 3-6 August 2012. National Hurricane Center (nhc.noaa.gov/data/tcr/AL062012_Florence.pdf)

Carlson TN (1969) Some remarks on African disturbances and their progress over the tropical Atlantic. Mon Wea Rev 97:716–726

Carlson TN, Prospero J (1972) The large-scale movement of Saharan air outbreaks over the northern equatorial Atlantic. J Appl Meteor 11:283–297

Cecelski SF, Zhang D-L (2013) Genesis of hurricane Julia (2010) within an African easterly wave: low-level vortices and upper-level warming. J Atmos Sci 70:3799–3817

Cecelski SF, Zhang D-L (2014) Genesis of hurricane Julia (2010) within an African easterly wave: Sensitivity analyses of WRF-LETKF ensemble forecasts. J Atmos Sci 71:3180–3201

Charney JG, Stern M (1962) On the stability of internal baroclinic jets in a rotating atmosphere. J Atmos Sci 19:1165–1184

Chen SH, Wang S, Waylonis M (2010) Modification of Saharan air layer and environmental shear over the eastern Atlantic Ocean by dust-radiation effects. J Geophys Res. doi:10.1029/2010JDO14158

Diedhiou A, Janicot S, Viltard A, de Felice P (1998) Evidence of two regimes of easterly waves over West Africa and the tropical Atlantic. Geophys Res Lett 25:2805–2808

Dunion JP, Velden C (2004) The impact of the Saharan air layer on Atlantic tropical cyclone activity. Bull Amer Meteor Soc 85:353–365

Estoque MA, Lin M (1977) Energetics of easterly waves. Mon Wea Rev 105:582–589

Fjortoft R (1950) Application of integral theorems in deriving criteria of stability for laminar flows and for the baroclinic circular vortex. Geofis Publ 17(6):5–52

Frank NL (1970) Atlantic tropical systems of 1969. Mon Wea Rev 98:307–314

Holton JR (1971) A diagnostic model for equatorial wave disturbances: the role of vertical shear of the mean zonal wind. J Atmos Sci 28:55–64

Hsieh JS, Cook K (2005) Generation of African easterly wave disturbances: relationship to the African easterly jet. Mon Wea Rev 133:1311–1327

Hsieh JS, Cook K (2007) A study of the energetics of African easterly waves using a regional climate model. J Atmos Sci 64:421–440

Hsieh JS, Cook K (2008) On the instability of the African easterly jet and the generation of African waves: reversals of the potential vorticity gradient. J Atmos Sci 65:2130–2151

Karyampudi VM, Carlson T (1988) Analysis and numerical simulations of the Saharan air layer and its effect on easterly wave disturbances. J Atmos Sci 45:3102–3136

Karyampudi VM, Carlson T, Pierce H (2002) Synoptic-scale influence of the Saharan air layer on tropical cyclogenesis over the eastern Atlantic. Mon Wea Rev 130:3100–3128

Kwon HJ (1989) A re-examination of the genesis of African waves. J Atmos Sci 46:3621–3631

Lorenz EN (1955) Available potential energy and the maintenance of the general circulation. Tellus 7:157–167

Norquist DC, Recker E, Reed R (1977) The energetics of African wave disturbances as observed during Phase III of GATE. Mon Wea Rev 105:334–342

Oort AH (1964) On estimates of the atmospheric energy cycle. Mon Wea Rev 92:483–493

Reed RJ, Norquist D, Recker E (1977) The structure and properties of African wave disturbances as observed during Phase III of GATE. Mon Wea Rev 105:317–333

Rennick MA (1976) The generation of African easterly waves. J Atmos Sci 33:1955–1969

Riehl H (1954) Tropical Meteorology. McGraw-Hill, pp 392

Rosenfeld D, Woodley W, Khain A, Cotton W, Carrio G, Ginis I, Golden J (2012) Aerosol effects on microstructure and intensity of tropical cyclones. Bull Amer Meteor Soc 93:987–1001

Schubert WH, Ciesielski P, Stevens D, Kuo H (1991) Potential vorticity modeling of the ITCZ and the Hadley circulation. J Atmos Sci 48:1493–1509

Thorncroft CD, Hodges K (2001) African easterly wave variability and its relationship to Atlantic tropical cyclone activity. J Climate 14:1166–1179

Thorncroft CD, Hodges K, Hoskins B (1994a) An idealized study of African easterly waves. Part I: a linear view. Quart J Roy Meteor Soc 120:953–982

Thorncroft CD, Hodges K, Hoskins B (1994b) An idealized study of African easterly waves. Part II: a nonlinear view. Quart J Roy Meteor Soc 120:983–1015

Zhang H, McFarquhar G, Cotton W, Deng Y (2009) Direct and indirect impacts of Saharan dust acting as cloud condensation nuclei on tropical cyclone eyewall development. Geophys Res Lett 36:L06802. doi:10.1029/2009GL037276